THE JOURNAL OF PHYSICAL CHEMISTRY B

Article

pubs.acs.org/JPCB

Exploring the Aqueous Vertical Ionization of Organic Molecules by Molecular Simulation and Liquid Microjet Photoelectron Spectroscopy

Peter R. Tentscher,[†] Robert Seidel,[‡] Bernd Winter,[§] Jennifer J. Guerard,[†] and J. Samuel Arey*[,†,∥]

[†]Environmental Chemistry Modeling Laboratory, GR C2 544, Ecole Polytechnique Fédérale de Lausanne, Station 2, CH-1015 Lausanne, Switzerland

[‡]Department of Chemistry, University of Southern California, 920 Bloom Walk, Los Angeles, California 90089-0482, United States

[§]Institute of Methods for Material Development, Helmholtz Center Berlin for Materials and Energy, Albert-Einstein-Strasse 15, 12489 Berlin, Germany

[∥]Department of Environmental Chemistry, Eawag, Swiss Federal Institute of Aquatic Science and Technology, Überlandstrasse 133, CH-8600 Dübendorf, Switzerland

Supporting Information

ABSTRACT: To study the influence of aqueous solvent on the electronic energy levels of dissolved organic molecules, we conducted liquid microjet photoelectron spectroscopy (PES) measurements of the aqueous vertical ionization energies (VIE_{aq}) of aniline (7.49 eV), veratrole alcohol (7.68 eV), and imidazole (8.51 eV). We also reanalyzed previously reported experimental PES data for phenol, phenolate, thymidine, and protonated imidazolium cation. We then simulated PE spectra by means of QM/MM molecular dynamics and EOM-IP-CCSD calculations with effective fragment potentials, used to describe the aqueous vertical ionization energies for six molecules, including aniline, phenol, veratrole alcohol, imidazole, methoxybenzene, and dimethylsulfide. Experimental and computational data enable us to decompose the VIE_{aq} into elementary processes. For neutral compounds, the shift in VIE upon solvation, ΔVIE_{aq}, was found to range from ≈−0.5 to −0.91 eV. The ΔVIE_{aq} was further explained in terms of the influence of deforming the gas phase solute into its solution phase conformation, the influence of solute hydrogen-bond donor and acceptor interactions with proximate solvent molecules, and the polarization of about 3000 outerlying solvent molecules. Among the neutral compounds, variability in ΔVIE_{aq} appeared largely controlled by differences in solute−solvent hydrogen-bonding interactions. Detailed computational analysis of the flexible molecule veratrole alcohol reveals that the VIE is strongly dependent on molecular conformation in both gas and aqueous phases. Finally, aqueous reorganization energies of the oxidation half-cell ionization reaction were determined from experimental data or estimated from simulation for the six compounds aniline, phenol, phenolate, veratrole alcohol, dimethylsulfide, and methoxybenzene, revealing a surprising constancy of 2.06 to 2.35 eV.

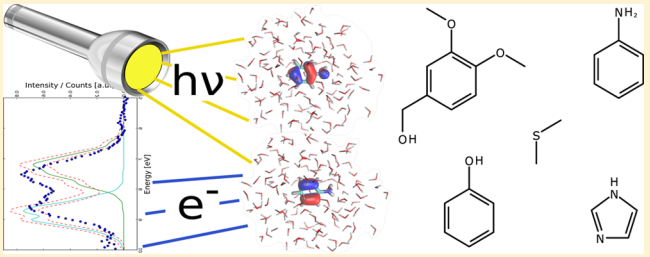

INTRODUCTION

Organic reactions in aqueous solution[1] are a central topic in the biochemical sciences,[2] in aquatic environmental chemistry,[3,4] water treatment,[5−7] and in the study of cloud droplets[8] and other hydrated aerosols.[9] The reactivities of organic chemicals in aqueous solution are determined by their solvated electronic structure. The most direct measurement of electronic energy levels is the determination of electron binding energies by means of photoelectron spectroscopy (PES), which has been applied to gas phase molecules, clusters, solids, and surfaces for decades.[10,11] From a chemist's perspective, the valence region of the PE spectrum is of utmost interest, since it contains the energy levels of the valence electrons taking part in chemical transformations.

Only recently was the concept of PE spectra transferred from the gas phase into the bulk aqueous solution. With the introduction of the aqueous microjet technique,[12−14] it became possible to measure PE spectra of solvated molecules in an aqueous microjet of about 24 μm diameter. This technique scans multiple spectral bands, each of which correspond to the ejection of single valence electrons from different energy levels of the solvated molecule. Thus, it allows the direct observation of the effects of solvation on the valence electronic structure of the solutes. Aqueous valence PE spectra have been published for several inorganic species,[15−23] but data on organics are limited to a few molecules: imidazole,[24] protonated imidazolium,[25] thymidine,[26] cytidine,[26] phenol,[27] and phenolate.[27] In a differential spectrum, from which the water solvent background

Received: August 8, 2014
Revised: November 20, 2014
Published: December 17, 2014

has been subtracted, the lowest energy PE band corresponds to the first valence vertical ionization energy, VIE_{aq}. Throughout this article, the second and third lowest energy ionizations are referred to as $VIE_{2,aq}$ and $VIE_{3,aq}$, respectively. The experimental determination of $VIE_{i,aq}$ by this manner is greatly facilitated if $VIE_{i,aq}$ is lower in energy than the $1b_1$ water band onset, which is the case for $VIE_{1,aq}$ of the compounds studied here.

The VIE_{aq} is directly related to the reorganization energy, λ_{aq}, of a one-electron oxidation half-cell reaction, as illustrated by the thermodynamic cycle in Figure 1:

$$\lambda_{aq} = VIE_{aq} - AIE_{aq}$$
$$AIE_{aq} = F(E_{h,i} + E_{h,SHE} - 0.03261V) \quad (1)$$

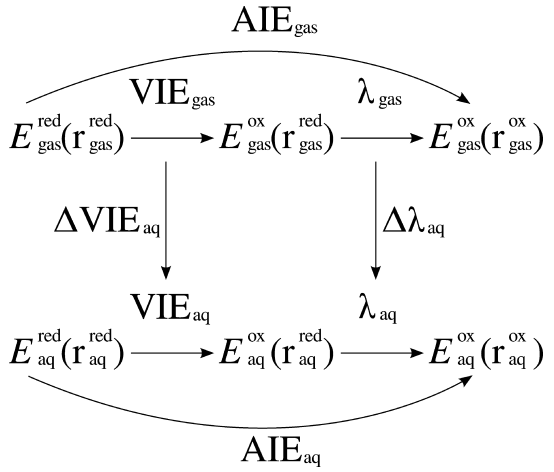

Figure 1. Schematic overview of vertical and adiabatic ionization processes in the aqueous phase (bottom) and the gas phase (top). Energies $E_{medium}^{oxidation\ state}$ depend on the geometrical coordinate $r_{medium}^{oxidation\ state}$.

where AIE_{aq} is the adiabatic ionization energy in aqueous solution, $E_{h,i}$ is the free energy of reaction of compound i with the standard hydrogen electrode (SHE), the latter having an absolute potential of $E_{h,SHE}$, and F is the Faraday constant. Note that the AIE_{aq} differs from the standard oxidation potential $E_{h,i}$ in that (i) AIE_{aq} is a free energy of reaction, that is, not referenced to the SHE; and (ii) the ejected electron is described within the ion convention, which adds a constant −0.03261 eV to the AIE_{aq}.[28] As discussed in earlier work,[19,29,30] the above definition of λ_{aq} is general; in other words it is not restricted to the linear response approximation (LRA) employed in Marcus theory. In eq 1 we have ignored the small potential difference between solution and vapor phase.[19] The reorganization energy, λ_{aq}, corresponds to the energy required to deform the ionized solute + solvent system from its equilibrium geometry to the geometry of the nonionized state. We may thus consider a two-step process: (i) a one-electron oxidation at the nonionized system geometry, and (ii) the subsequent relaxation of the geometry of the ionized system, freeing $-\lambda_{aq}$.

We can imagine these processes to take place either in solution or in the gas phase, as summarized in Figure 1 for the oxidation half-cell reaction. Thus, we may express the effect of solvation on the quantities VIE, AIE, and λ, as

$$\Delta VIE_{aq} = VIE_{aq} - VIE_{gas} \quad (2)$$

$$\Delta AIE_{aq} = AIE_{aq} - AIE_{gas} \quad (3)$$

$$\Delta\lambda_{aq} = \lambda_{aq} - \lambda_{gas} \quad (4)$$

Consequently, the vertical ionization, adiabatic ionization, and reorganization processes can each be separated into a gas phase and a solution phase component. The ΔVIE_{aq}, ΔAIE_{aq}, and $\Delta\lambda_{aq}$ represent the change in vertical ionization energy, adiabatic ionization energy, and reorganization energy, respectively, upon moving from the gas phase into the aqueous phase.

Within the Marcus linear response approximation, the vertical ionization energy can be used to compute the adiabatic ionization energy of a one-electron oxidation in either gas or solution phase:[31,32]

$$AIE = \frac{VIE - VEA_{ox}}{2} \quad (5)$$

In eq 5, VIE is the lowest vertical ionization energy of the reduced species, for example, as measured by PES. VEA_{ox}, in contrast, is the vertical electron attachment energy of the oxidized radical species. Although VEA_{ox} has not been measured, it has been used in computation to estimate redox potentials of inorganic and organic compounds in solution.[31,32] Eq 5 assumes that λ is identical for both the oxidation step and the (reverse) reduction step of a half-reaction. The VIE is further connected to the Marcus theory of electron transfer in the condensed phase, in which the outer sphere electron transfer (ET) rate constant, k_{et}, may be estimated from the free energy of reaction of the redox pair, ΔG_{rxn}, and the reorganization energy of reaction, λ_{rxn}:[33−35]

$$k_{et} = \frac{2\pi}{\hbar}|H_{AB}|^2 \frac{1}{\sqrt{4\pi\lambda_{rxn}k_bT}} e^{-(\lambda_{rxn}+\Delta G_{rxn})^2/4\lambda_{rxn}k_bT} \quad (6)$$

where H_{AB} is the electronic coupling element between the reactant state A and the product state B, k_b is the Boltzmann constant, and T is the temperature.

Any computational protocol aiming at the estimation of redox potentials should be able to reproduce the VIE of a solvated molecule, if not its entire valence PE spectrum. To test such computational protocols, we compare computed VIE_{aq} distributions with experimental PE spectra for diverse organic molecules. To date, given the scarce number of organic molecules for which aqueous PE spectra have been reported, this is hardly possible.

In the present contribution, our goals are 3-fold. First, we extend the set of experimentally available valence PE spectra of organic molecules in an aqueous microjet, enlarging the available collection of aqueous vertical ionization energy (VIE_{aq}) and half-cell reorganization energy (λ_{aq}) values. Second, we aim at the computational reproduction of the measured PE energy levels, using state-of-the-art simulation methodologies. Third, we explore and interpret the physical processes that influence vertical ionization energies in solution, based on analysis of the combined set of experimental and simulation data. These findings advance our insights into the role of aqueous solvation during the oxidation process, and they also contribute to the development and testing of computational methodologies for simulation of one-electron oxidations of organic solutes in aqueous solution.

dx.doi.org/10.1021/jp508053m | J. Phys. Chem. B 2015, 119, 238−256

EXPERIMENTAL SECTION

Solutions of aniline, methoxybenzene, veratrole alcohol, and imidazole were prepared in highly deionized water (18 MΩ cm^{-1}). All solutions, including the reference water sample, contained 40−50 mmol kg^{-1} NaF to counter charging effects. Electron emission from the salt does not contribute to binding energies lower than 10 eV, and furthermore, all of our previous studies on many aqueous solutions have shown no measurable counterion effects on both the solvent and the solute photoelectron spectra at this rather low concentration. We do not expect direct interactions of the ions with the neutral organics measured, which would require close contact/complexation. The solubility of the studied organic compounds was limited, resulting in molal compositions as follows: aniline 127 mmol kg^{-1}, pH = 8.5; methoxybenzene 10 mmol kg^{-1}, pH = 7.4; veratrole alcohol 15 mmol kg^{-1}, pH = 8.0; imidazole, 2000 mmol kg^{-1}, pH = 10.25.

Valence photoemission measurements of these solutions were performed at the undulator beamline U41-PGM of the BESSY II synchrotron facility, Berlin. Photoelectron (PE) spectra were recorded from a 24 μm liquid microjet of the solutions, injected into vacuum with a velocity of 50 m s^{-1} (backing pressure ≈ 5 bar). The reservoir temperature was up to 293 K. The jet temperature in the interaction region was previously estimated to be around 283 K by evaporative cooling modeling.[14] The details of the experimental setup are described elsewhere.[12,13,27] The photon energy was 200 eV, and the energy resolution was ≈100 meV. Reported spectra are calibrated to the water $1b_1$ peak (11.16 eV binding energy) and normalized to the (storage) ring current of BESSY. The reported spectra are differential spectra from which the solvent spectrum has been subtracted. The temperature in the aqueous microjet may not be well-defined. However, the resulting ionization energies are treated as ionization at 298 K for the purposes of comparison to experimental adiabatic data (Figure 1) and simulations carried out at 298 K.

COMPUTATIONAL DETAILS

Gas Phase Ionization Energies. *Stationary Geometry Structures.* All calculations were performed with Gaussian09, Rev. B.1.[36] Structures of both closed-shell and open-shell (oxidized) organic molecules were geometry optimized with the B2PLYPD[37] double hybrid functional together with Ahlrich's tzvpp[38] basis set. The basis for heteroatoms (N, O, S) was augmented with diffuse functions from Dunning's aug-cc-pVTZ[39] basis set. This is referred to as (partially augmented) pa-tzvpp. For phenolate and phenoxyl radical, all centers included augmented basis sets (aug-tzvpp) to accommodate the negative charge on phenolate. For the structures of thymidine and its radical cation, Pople's 6-311+G(d,p) basis set[40] was used instead to decrease computational cost. The nature of structures (minimum, saddle point) was confirmed by harmonic normal-mode analysis.[41] On these structures, single point calculations were performed with different electronic structure methods to determine AIE_{gas} and VIE_{gas} values, explained below.

AIE_{gas} Values. Adiabatic ionization energy calculations were performed with B2PLYPD, employing Ahlrich's qzvpp[38] basis set further augmented by diffuse functions from Dunning's aug-cc-pVQZ[39] basis, denoted aug-qzvpp throughout the article. Additional calculations were performed with several composite methods: ROCBSQB3,[42] W1RO,[43] W1U,[44] and W1BD.[44] For all composite methods, structures were not geometry-optimized with the respective associated methods; geometries were instead obtained from B2PLYPD calculations as discussed above. Based on a previous assessment of radical geometries and vibrational frequencies,[45] we believe that the B2PLYPD structures and vibrational frequencies are superior to their B3LYP counterparts with which these composite methods were designed. Throughout the article, (RO)-CBSQB3 and the different W1 methods always refer to electronic energy calculations with the composite protocol, using the structures and harmonic frequencies from the B2PLYPD calculations.

We preferred W1BD energies as reference results, although W1RO was preferred when remaining spin contamination was present or when W1BD was not computationally affordable. For the VIE computation on phenolate, neither of these methods converged, and W1U was used instead. For thymidine, ROCBSQB3 was not affordable. The reported results correspond to the ROCBSQB3 data for thymine, plus the difference between thymine and thymidine ionization energies evaluated by B2PLYPD.

Calculated AIE_{gas} values are given at 0 K, including harmonic zero-point vibrational energies, to allow direct comparison to available experimental data. Temperature contributions (298 K) to the AIE_{gas}, reported separately as ΔG_{rotvib}, are given as the difference between the electronic ionization energy and the ionization energy at 298 K. These are rotational and vibrational contributions to the free energies, accounted for by using the rigid rotor and harmonic oscillator approximations.[46]

VIE_{gas} Values. VIE_{gas} values were calculated on the optimized geometry of the respective closed-shell molecule, and are reported as differences in electronic energies between the ionized and reduced states. To diagnose for temperature (vibrational) effects on the VIE_{gas}, we performed VIE_{gas} calculations on a minimum energy structure and also on a single vibrationally averaged structure as follows. Geometries were optimized with the B3LYP/pa-tzvpp model chemistry. In additional calculations with the same model chemistry, vibrationally averaged geometries were calculated (298 K) using the VPT2[47] protocol. On both structures, the VIE_{gas} values were calculated with the B3LYP/pa-tzvpp model chemistry. The difference is reported as

$$\Delta VIE_{vib.av.} = VIE_{vib.av.} - VIE_{stationary} \quad (7)$$

Solute−Water Binary Complexes. The geometries of binary clusters between closed-shell organic molecules and water were optimized in a cluster-continuum scheme. The M06L[48]/aug-cc-pVDZ model chemistry was used to optimize each solute-water binary cluster, and the SMD[49] aqueous solvation model was employed to account for solvation of the cluster. All structures of binary clusters were confirmed to be energetic minima by normal-mode analysis. On these cluster geometries, gas phase binding energies between solute and water molecule were calculated with the (RO)BHandHLYP[50]/aug-cc-pVTZ[39] model chemistry, using the counterpoise correction[51] throughout. Intermolecular interactions involving radicals can differ from those of analogous closed shell systems,[52] and the above model chemistries were selected based on their good performance in our recent assessment of weak interactions involving radicals with polar molecules such as water.[53] In additional calculations, the binding energy calculations were repeated using identical geometries, but in the n^{-1} electron (oxidized) configuration:

dx.doi.org/10.1021/jp508053m | J. Phys. Chem. B 2015, 119, 238−256

$$\Delta \mathrm{VIE}_{1\cdot \mathrm{H_2O}} = \mathrm{VIE}_{1\cdot \mathrm{H_2O}} - \mathrm{VIE}_{\mathrm{gas}}$$
$$= E^{n-1}_{1\cdot \mathrm{H_2O}} - E^{n}_{1\cdot \mathrm{H_2O}} - (E^{n-1}_{\mathrm{gas}} - E^{n}_{\mathrm{gas}})$$
$$= E^{n-1}_{\mathrm{bind}} - E^{n}_{\mathrm{bind}} \quad (8)$$

In eq 8, E^n denotes the electronic energy of the n-electron configuration of the system.

Gas Phase Conformational Analysis for ODMB and Veratrole Alcohol. For *o*-dimethoxybenzene and veratrole alcohol, we analyzed the rotamers associated with the rotation of the methoxy group (and the orientation of the $-CH_2OH$ group for veratrole alcohol) relative to the aromatic ring in the gas phase. Gibbs free energies were computed based on (RO−)CBSQB3 electronic energies with B2PLYPD/pa-tzvpp structures, including thermal effects based on vibrational and rotational data from B2PLYPD/pa-tzvpp computations. Relative Gibbs free energies, ΔG_{conf}, are given with respect to the most stable conformer. ΔG_{conf} values are reported for each stationary structure, and a degeneracy term g describes the contribution to the Boltzmann distribution of the ΔG_{conf} value.

For veratrole alcohol, many stable conformers exist in the gas phase: the -OCH_3 groups assume three different configurations, *trans*, *gauche*, and *all-gauche*, in analogy to ODMB. Additionally, the internal rotation of the $-CH_2OH$ group visits four minima during a full turn. For each of those, the −OH group can point away from the aromatic ring, or point toward the aromatic ring ("in" and "out", respectively). This results in n = 28 unique conformers of C_1 symmetry. Each of these unique conformers are two-fold degenerate (g = 2), with the degenerate systems behaving like stereoisomers of each other. The population of each conformer was determined using a Boltzmann distribution according to the computed ΔG_{conf} values. We grouped these conformers, and we report weighted average values and weighted standard deviations for the Gibbs free energies (with respect to the most stable conformer) and VIEs. The averaging is again based on weights from the Boltzmann distribution of the individual ΔG_{conf} values.

The tabulated VIE and AIE values of veratrole alcohol were calculated as follows. For the total VIE at T = 298 K, the VIEs of the 28 conformers were considered with their respective Boltzmann populations (weighted average). The small temperature effects ($\Delta \mathrm{VIE}_{\mathrm{vib.av.}}$) were not considered. The AIE at T = 0 K was based on the lowest energy conformer of both the neutral and the radical cation species. For the AIE at T = 298 K, conformers of both the neutral (n = 28) and the radical cation (n = 2) system were considered:

$$\mathrm{AIE}_{\mathrm{gas,298K}} = \sum^{n_{\mathrm{ox}}} w_{\mathrm{ox}} \Delta G_{\mathrm{conf,ox}} - \sum^{n_{\mathrm{red}}} w_{\mathrm{red}} \Delta G_{\mathrm{conf,red}} \quad (9)$$

n_{ox} (n_{red}) is the number of considered conformers of the radical cation (neutral) system, w_{ox} (w_{red}) is the Boltzmann weight of each conformer, and ΔG_{conf} is the free energy change with respect to the lowest energy conformer of the oxidized (reduced) manifold. For the radical cation, B2PLYPD geometry optimizations yielded *trans-out* as the only stable conformers, with the −OH group in the ring plane (C_s symmetry). For the purely computational decomposition of $\Delta \mathrm{VIE}_{\mathrm{aq}}$ to $\Delta \mathrm{VIE}_{\mathrm{aq/def/hyd}}$ of the individual conformers (described below by eqs 13−15), $\mathrm{VIE}_{\mathrm{gas}}$ values of the individual conformers were computed at the EOM-IP-CCSD level (see below), and these values were used together with the corresponding CBSQB3-based Boltzmann weights.

In addition to calculations of local minima, a potential energy surface scan of the out-of-plane rotation of one of the methoxy groups of ODMB was performed. That is, the dihedral angle d_{COCC} was held fixed, while the rest of the system was allowed to relax for incrementally varied values of the d_{COCC} dihedral. Resulting partially constrained geometry optimizations were obtained with the BLYP-D2[59]/aug-cc-pVDZ[39] model chemistry, using Gaussian09, Rev D.1. On these structures, $\mathrm{VIE}_{\mathrm{gas}}$ values were computed with EOM-IP-CCSD[68] with 6-31+G* and aug-cc-pVDZ basis sets, using Q-Chem 4.0.1.0.[67]

Aqueous QM/MM Molecular Dynamics. Molecular dynamics (MD) simulations of aqueous solutes were pre-equilibrated employing a classical potential with AMBER 11,[54] using the GAFF[55] to describe the solute and the polarizable POL3[56] force field for solvent molecules. A 55 × 55 × 55 Å cubic box with periodic boundary conditions was used. In both classical MD and the subsequent QM/MM MD simulations, the geometries of water molecules were constrained using the SHAKE algorithm.[57]

QM/MM MD simulations were performed with the CP2K[58] software package. Aqueous solvent was represented by the classical polarizable POL3[56] force field. The organic solute was represented quantum mechanically as follows. We used the BLYP functional with Grimme's D2 dispersion correction,[59] where the core electrons were represented by GTH pseudopotentials,[60] and the valence electrons were represented by a Gaussian and plane waves (GPW) setup.[61,62] The cutoff for the plane waves was set to 300 Ry, and the TZVPP basis set optimized for GTH pseudopotentials was used. The convergence criterion of the electronic energy was set to 1×10^{-6} E_h. The box size of the MM region was 55.131 × 55.131 × 55.131 Å^3, and the box size of the QM region was 13.425 × 13.425 × 13.425 Å^3 for all systems, except for the larger veratrole alcohol system, where the size of the QM region was 16.0 × 16.0 × 16.0 Å^3. Periodic boundary conditions were used. The coupling between the QM region and the MM region is described elsewhere.[63,64] As the same MM box dimensions were employed for dynamics simulations of each solute, the number of water molecules in the periodic box varied from 4885 to 4884, depending on the size of the solute. Separately chained Nosé−Hoover thermostats were used for the QM and the MM regions, with chain lengths of three and time constants of 1000 in both cases. QM/MM MD was performed in the NVT ensemble at T = 300 K with an integration time step of 0.5 fs. The total simulation time was 30 ps, of which the first 5 ps was considered an equilibration period and was excluded from further analysis.

Additional gas phase MD simulations were performed on veratrole alcohol with Q-Chem 4.0.1.0. These NVE simulations used the BLYP-D2/6-31G* model chemistry, a time step of 0.48 fs, and an SCF convergence of 1×10^{-6} E_h.

Aqueous Phase VIE Computations. $\mathrm{VIE}_{\mathrm{aq}}$ calculations were performed with a QM/effective fragment potential (EFP)[65,66] scheme as implemented in Q-Chem 4.0.1.0.[67] From each production MD trajectory of 25 ps length, 499 system geometries ("snapshots") were extracted at equidistant (50 fs) time intervals. Autocorrelation analysis of the snapshot $\mathrm{VIE}_{\mathrm{aq}}$ values confirmed that these time series data were mutually independent. Using the solute−solvent conformations from these snapshots, VIE calculations of microsolvated clusters of different sizes were performed, where each cluster was centered on the organic solute. These included (a) a gas phase VIE calculation with the EOM-IP-CCSD[68]/6-31+G* model

dx.doi.org/10.1021/jp508053m | J. Phys. Chem. B 2015, 119, 238−256

chemistry and (b) VIE calculations on clusters containing 32, 64, 128, 256, 384, 1024, 3072, and 4096 explicit water molecules. In cases where the cluster boundary exceeded the dimensions of the MD box, water molecules from the PBC mirror images were used. This affected the clusters having 3072 and 4096 water molecules.

A stiff, fixed geometry EFP model of water from the Q-Chem EFP library was used. This was superimposed onto the (also fixed geometry) POL3 water molecules from the QM/MM MD trajectory by minimizing the squared deviation of the absolute coordinates in all three centers, for all waters in the cluster.

Calculation of Redox Quantities. $AIE_{aq,298K}$ values were calculated from experimental one-electron redox potentials using eq 1. An absolute potential of the standard hydrogen electrode of 4.28 V[69] was used together with a Faraday constant of F = 96485.3365 C mol^{-1}. $\lambda_{aq,298K}$ was computed by eq 1, based on $AIE_{aq,298K}$ data and VIE_{aq} values derived from aqueous microjet PE spectra. $AIE_{gas,298K}$ was calculated as the sum of the electronic energy difference between the oxidized and reduced species and the corresponding ΔG_{rotvib}. $VIE_{gas,298K}$ was calculated as the sum of appropriate electronic energy difference and $\Delta VIE_{vib.av.}$. $\lambda_{gas,298K}$ was calculated as $VIE_{gas,298K} - AIE_{gas,298K}$, analogous to eq 1.

Data Processing for Simulated Aqueous PE Spectra. *Gas Phase Correction to the Aqueous VIE Values.* A collection of VIE_{aq} values was obtained, using the EOM-IP-CCSD/6-31+G* model chemistry to describe the solute coupled with EFPs to describe solvent water molecules. To correct for systematic errors in VIE_{aq} data computed by EOM-IP-CCSD/6-31+G*, we performed additional EOM-IP-CCSD/6-31+G* calculations of VIE_{gas} on the gas phase stationary structure of the solute obtained with B2PLYPD/pa-tzvpp. The difference in VIE_{gas} computed with EOM-IP-CCSD/6-31+G* and VIE_{gas} computed with the reference method (W1 or ROCBSQB3, denoted *reference* below) was subsequently added to the ensemble of computed QM/EFP VIE_{aq}, $VIE_{2,aq}$, and $VIE_{3,aq}$ values:

$$\begin{aligned}
VIE^{cluster}_{1,aq,corrected} &= VIE^{cluster}_{1,aq,EOMIP-CCSD} \\
&\quad - VIE^{stationary}_{1,gas,EOMIP-CCSD} + VIE^{stationary}_{1,gas,reference} \\
VIE^{cluster}_{2,aq,corrected} &= VIE^{cluster}_{2,aq,EOMIP-CCSD} \\
&\quad - VIE^{stationary}_{1,gas,EOMIP-CCSD} + VIE^{stationary}_{1,gas,reference} \\
VIE^{cluster}_{3,aq,corrected} &= VIE^{cluster}_{3,aq,EOMIP-CCSD} \\
&\quad - VIE^{stationary}_{1,gas,EOMIP-CCSD} + VIE^{stationary}_{1,gas,reference}
\end{aligned} \tag{10}$$

For the simulated aqueous PE spectra, the negligible vibrational effects on the $VIE_{i,gas}$ values were omitted. For the simulated aqueous PE spectrum of veratrole alcohol, the conformers were not treated independently, and the resulting spectrum corresponds to the conformer populations as predicted by the BLYP-D2 model chemistry used for the MD simulation. The gas phase correction to the entire veratrole spectrum as shown in eq 10 was carried out using data for the *trans-out* conformer.

For the partitioning of the $\Delta VIE_{aq,comp}$ into different components, three conformers of veratrole alcohol were considered separately. The snapshots of the MD trajectory were attributed to three conformers: *trans* if both $d_{COCC} < 70°$, *gauche* if one $d_{COCC} > 70°$, and *all-gauche* if both $d_{COCC} > 70°$. By averaging over these regions in dihedral angle space, mean aqueous values for the individual conformers were obtained. These were combined with the corresponding conformer-specific gas-phase data (see above) to enable partitioning for the individual species independently of the conformer populations predicted by the MD protocol.

Data Smoothing of the Simulated VIE_{aq} Distribution. The limited number (499) of solvated cluster snapshots did not lead to smooth histogram shapes for the simulated VIE_{aq}. Therefore, we smoothed the distribution of VIE_{aq} values with kernel density estimation.[70] For each VIE contributing to the spectrum, a Gaussian kernel of the form:

$$K = \frac{1}{\sqrt{2\pi}} e^{-\frac{\Delta x^2}{h}} \tag{11}$$

was used. The bandwidth h was selected assuming a Gaussian distribution of the data:

$$h = 1.06 \cdot \sigma \cdot n^{-1/5} \tag{12}$$

where σ is the standard deviation of the VIE_{aq} distribution and n is the number of snapshots. This produces a smoothed distribution of each vertical ionization, labeled as VIE_{aq}, $VIE_{2,aq}$, or $VIE_{3,aq}$ in Figure 8. For the smoothing of the complete spectrum, used for sampling error estimation (below), the largest bandwidth h encountered in the simulated distributions was used.

Estimation of the Sampling Error of the Simulated VIE_{aq} Distribution. Autocorrelation analysis of the MD trajectories revealed that the 499 samples taken were mutually uncorrelated. The sampling error of each averaged VIE_{aq} value was estimated to be ≈0.02 eV. In order to estimate the uncertainties in the VIE_{aq} distributions arising from finite sampling, we used a bootstrap/resampling approach.[71] Resampling was applied to the total ensemble of VIE_{aq} snapshots contributing to the simulated PE spectrum. The total VIE_{aq} distribution was resampled with replacement 10^5 times. For each synthetic sample, the kernel density was estimated by eq 11, using h (eq 12) as determined for the original data. The mean VIE_{aq} values of the synthetic sample set were visually indistinguishable from the original smoothed VIE_{aq} distribution. In Figure 8, at each value of the distribution, we show a band enveloping the 95% confidence interval (2σ) of the mean of the synthetic sample set.

RESULTS AND DISCUSSION

Selection of Organic Molecules Studied. We aim to explore the effects of aqueous solvation on the vertical ionization energy (VIE_{aq}) and the half-cell reorganization energy (λ_{aq}) of a diverse set of organic compounds. We report new experimental and simulated aqueous photoelectron spectra for aniline, veratrole alcohol, methoxybenzene, and imidazole. We also simulated the aqueous PE spectrum of phenol and compared these data to previously reported experimental aqueous PES data. For two compounds, aniline and veratrole alcohol, accurate aqueous oxidation potentials are also available, as determined previously by pulse radiolysis. This allows us to deduce half-cell reorganization energies for these two compounds. Finally, a simulated aqueous PE spectrum is reported for dimethylsulfide (DMS). DMS and methoxybenzene allow us to explore the role of hydrogen bond accepting moieties on the vertical ionization process. Additionally, calculations were conducted to predict the gas phase ionization

dx.doi.org/10.1021/jp508053m | J. Phys. Chem. B 2015, 119, 238−256

Table 1. Experimental and Computed Adiabatic (AIE_{gas}) and Vertical (VIE_{gas}) Gas Phase Ionization Energies of Organic Molecules (eV)

	aniline	phenol	imidazole	methoxybenzene	dimethylsulfide	thymine	*o*-dimethoxybenzene[a]	phenolate	imidazolium	veratrole alcohol[a]	thymidine[f]
					adiabatic ionization energies						
computed vibrational and rotational contributions to AIE_{gas} (298 K)											
ΔE_{ZPVE}	0.026	0.009	−0.021	−0.001	−0.037	−0.033	0.018	0.026	−0.053	0.015	−0.061
ΔG_{rotvib}	0.010	−0.011	−0.040	−0.025	−0.075	−0.067	−0.003	0.007	−0.072	0.036	−0.104
computed AIE_{gas} at 0 K											
W1BD	7.752	8.542	8.841		8.692				15.063		
W1RO	7.744		8.833	8.257				2.259[d]	15.057		
ROCBSQB3	7.760	8.584	8.858	8.306		8.953	7.704	2.244[e]	15.068	7.484	8.325
B2PLYPD	7.569	8.342	8.787	8.321		8.841	7.390	2.299	15.010		8.214
experimental AIE_{gas} at 0 K											
AIE_{gas}	7.7206	8.5088	8.66−8.81	8.2324	8.6903	8.9178	7.6395	2.2538			
M.U.[b]	0.0002	0.0005		0.0006	0.0009	0.0010	0.0006	0.0008			
method	ZEKE	ZEKE		ZEKE	MATI	MATI	MATI	PE			
ref.	77	78	74	79	80	81	82	83			
					vertical ionization energies						
computed temperature (vibrational) correction to VIE_{gas} (298 K)											
$\Delta VIE_{vib.av}$	−0.043	0.001	−0.008	−0.012	0.013	0.000	−0.005	0.005	−0.078		
computed VIE_{gas} at 298 K											
W1BD		8.751	9.109		8.811				15.296		
W1RO	8.038		9.102	8.467					15.293		
W1U								2.315			
ROCBSQB3	8.050	8.788	9.140	8.510		9.244	7.949	2.290	15.327	7.962	8.737
CBSQB3		8.781									
B2PLYPD	7.895	8.577	9.004	8.297		9.081	7.709	2.380	15.183		8.574
experimental VIE_{gas} at temperature											
VIE_{gas}	8.02−8.10	8.56−8.75	8.78−9.12	8.25−8.61	8.67−8.71	9.02−9.20	8.17[c]				
ref.	73	73	73,74	73,84	73	73	85				

[a]Except if noted otherwise, all data refer only to the most stable (*trans*) conformers of ODMB and veratrole alcohol. [b]Measurement uncertainty (M.U.), as reported in the original articles. [c]Experimental PE detachment energy of *o*-dimethoxybenzene involving several conformers, see text. [d]W1RO was nonconvergent for the radical species; spin-corrected W1U data is given instead. [e]ROCBSQB3 was nonconvergent for the radical species; regular CBSQB3 data is given instead. [f]Data computed on a single conformer, which may represent an underestimate of the conformer-averaged VIE_{gas}. See text for details.

dx.doi.org/10.1021/jp508053m | J. Phys. Chem. B 2015, 119, 238−256

properties of thymidine, phenolate, and protonated imidazolium, for which previously reported experimental aqueous phase PES data are available.

Gas-Phase Calculations. Before introducing aqueous phase data, we begin with a discussion of computed gas phase adiabatic ionization energy (AIE_{gas}) and vertical ionization energy (VIE_{gas}) values for all studied organic compounds, listed in Table 1. Gas phase computations enabled us to separate and attribute the effects of solvation on the vertical and adiabatic ionization processes (Figure 1). Below, we compare the quality of our modified CBSQB3 and W1 procedures to experimental AIE_{gas} and VIE_{gas} data, where available. Conformationally rigid molecules are discussed first. Veratrole alcohol and *o*-dimethoxybenzene (ODMB) both merit separate discussions, since these flexible molecules explore multiple stable conformations at 298 K. This applies to thymidine as well, but we did not perform a conformational analysis for this molecule (see below).

Quality of Computed AIE_{gas} and VIE_{gas} for Rigid Molecules. Our computed AIE_{gas} values exhibit good agreement with experiment for the rigid molecules phenolate, aniline, methoxybenzene, phenol, imidazole, imidazolium, thymine, and DMS. Thymine was viewed as an analogue for thymidine. The tabulated experimental AIE_{gas} data were measured previously by vibrationally resolved MATI and ZEKE methods. They refer to ionization at 0 K, including zero-point vibrational motion. With the exception of imidazole (discussed further below), the maximum absolute errors in computed AIE_{gas} values of the rigid molecules were 0.04 eV for the W1 and 0.08 eV for the ROCBSQB3 composite electronic structure methods (Table 1). Our modified ROCBSQB3 protocol agrees well with data produced by the original ROCBSQB3 protocol, which was evaluated recently for gas phase adiabatic ionization energies of a set of aromatic and aliphatic organic molecules.[72] The effects of temperature on AIE_{gas} are reported as ΔG_{rotvib}, defined as the change in the adiabatic ionization energy on going from 0 to 298 K. Vibrational effects are found to be only a minor contribution ($\leq$0.10 eV) to the computed AIE_{gas} values, irrespective of whether we consider ionization at 0 K or at 298 K.

Computed VIE_{gas} values agree with experiment to within the reported bounds of experimental variability for phenol, aniline, and methoxybenzene. Experimental VIE_{gas} values are deduced from gas phase PE spectra that are recorded at elevated temperature, usually at 60 to 70 °C. These experimental VIE_{gas} data exhibit a significant spread. In Table 1, the listed experimental data ranges correspond to values reported in the NIST webbook.[73] The computed VIE_{gas} values lie within 0.08 eV of these ranges, with the exception of imidazole (discussed further below). We performed VIE_{gas} calculations on both stationary as well as vibrationally averaged (VPT2) geometries at 298 K, and the VIE_{gas} difference is given as $\Delta VIE_{vib.av.}$ (Table 1). The contributions of $\Delta VIE_{vib.av.}$ are small ($\leq$0.08 eV) in all cases.

Finally, the experimental AIE_{gas} and VIE_{gas} values of imidazole are controversial topics, as recently summarized by Schwell et al.[74] Published adiabatic values are 8.66 and 8.81 eV, whereas published vertical values range from 8.78 to 9.12 eV. For a small molecule without conformational flexibility such as imidazole, the quantum chemical protocols employed by us should yield highly accurate results. Computations support an AIE_{gas} of 8.84 eV and a VIE_{gas} of 9.11 eV, respectively. It is worth noting that the assignment of experimental VIE_{gas} values is not unambiguous: in the PE spectrum of imidazole,[75,76] the first peak exhibits a pronounced fine structure, is non-Gaussian, and is tailing. The assignment of the experimental VIE_{gas} value thus depends on the type of data processing used.

Conformations of o-Dimethoxybenzene. The flexible molecule ODMB is a simpler analogue of veratrole alcohol, a compound for which we measured an aqueous photoelectron spectrum. According to previous reports[86] and also according to our own B2PLYPD calculations, three stable rotamers of ODMB exist in the gas phase, as shown in Figure 2. We

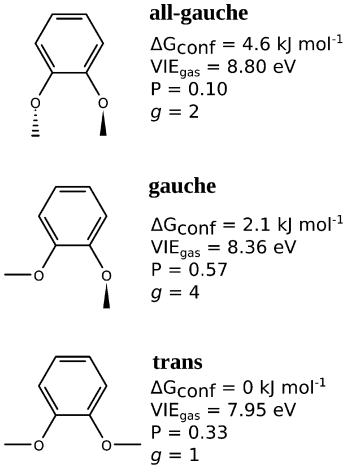

Figure 2. Stable gas phase conformers of *o*-dimethoxybenzene, shown together with the relative free energies of single conformers with respect to the lowest energy conformer (CBSQB3). Populations P are derived from Boltzmann statistics, using degeneracy numbers *g*. VIE_{gas} values are obtained from ROCBSQB3 calculations.

computed the Gibbs free energy difference of the conformers relative to the most stable (*trans*) conformer, labeled ΔG_{conf} in Figure 2, based on CBSQB3 electronic energies and B2PLYPD geometries and frequencies. The *trans* and *gauche* conformers are separated by only 2.1 kJ mol^{-1}, and thus, both conformers need to be considered in VIE_{gas} computations at 298 K. Using Boltzmann weighting of the conformer relative free energies and accounting for the degeneracies of each conformer, we predict the relative populations of the *trans*/*gauche*/*all-gauche* conformers to be 33:57:10% at 298 K. To allow direct comparison with experiment,[86] we repeated the calculations at the experimental temperature of 333 K, yielding a 32:58:10% distribution. This is in good agreement with the reported experimental distribution of 36(±16):50(±12):14 for *trans*, *gauche*, and *all-gauche* conformers, respectively.[86] It is challenging to make confident computational estimates of the relative populations of conformers having free energy differences as small as 2 kJ mol^{-1} to 3 kJ mol^{-1}. Nonetheless, these findings explain the gas phase photoelectron experiment for ODMB,[85] in which the reported VIE_{gas} of 8.17 eV lies approximately halfway between our computed VIE_{gas} values of the *trans* (7.95 eV) and *gauche* (8.36 eV) conformers. Considering its much higher VIE_{gas} of 8.80 eV, the *all-gauche* conformer would likely not significantly influence the peak maximum observed in the PE spectrum. A weighted average of the *trans* and *gauche* conformers yields a VIE_{gas} of 8.21 eV, close to the experimental peak maximum.

In Figure 3, we show the pronounced dependence of the three lowest vertical ionization energies, VIE_{gas}, $VIE_{2,gas}$, and $VIE_{3,gas}$, on the dihedral angle of one methoxy group relative to

dx.doi.org/10.1021/jp508053m | J. Phys. Chem. B 2015, 119, 238−256

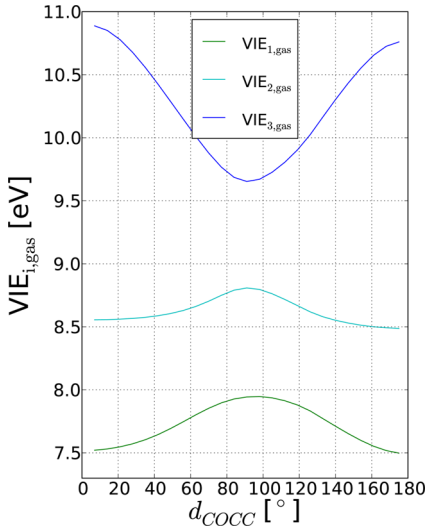

Figure 3. Three lowest VIE_{gas} values of ODMB as a function of the dihedral angle of the methoxy group relative to the aromatic ring, d_{COCC}. Values were computed with EOM-IP-CCSD/6-31+G* on geometries obtained by partly constrained optimization with BLYP-D2/aug-cc-pVDZ (the rotated d_{COCC} angle was held fixed).

the aromatic ring (d_{COCC}). With increasing nonplanarity ($d_{COCC} > 0$), both VIE_{gas} and $VIE_{2,gas}$ rise by several tenths of an eV, whereas $VIE_{3,gas}$ exhibits the opposite behavior. This means that interpeak distances in PE spectra can be influenced by varying conformer populations, highlighting the importance of accurate theoretical calculations for interpreting experimental PE spectrum data for flexible molecules.

The computed AIE_{gas} of ODMB of 7.68 eV is in excellent agreement with the experimental value[82] of 7.6395 ± 0.0006 eV. For the computation of AIE_{gas}, only the planar *trans* conformer was considered for both the neutral and oxidized radical cation species. The authors of the experimental study reported that only the *trans* conformer was observed. Although it is beyond the scope of the present study to determine why only one conformer was apparently observed in the AIE experiment, this may be explained by fast conformer interconversion (see SI). In the oxidized radical cation state, however, the trans conformer is clearly the only relevant species, as can be deduced from the VIE_{gas} values shown in Figure 2.

Conformations of Veratrole Alcohol. For veratrole alcohol, neither a gas phase PE spectrum nor experimental data concerning the populations of the gas phase conformers are available. Two types of conformers require consideration: (1) conformers arising from the deplanarization, in analogy to ODMB, and (2) conformers arising from the orientation of the $-CH_2OH$ group. The $-OH$ moiety can either point away from the aromatic ring (*out*), or toward the aromatic ring (*in*). Conformers with the OH group in the ring plane, as reported by Miller et al. for benzyl alcohol with the B3LYP functional,[87] were found to be transition states for veratrole alcohol with the B2PLYPD method. Throughout a full internal rotation of the $-CH_2OH$ group, four minima are visited, each of which exhibits stable *in*/*out* conformers. We considered a total of 28 unique conformers, each being 2-fold degenerate. Using the computed populations of all conformers, the average VIE_{gas} of veratrole alcohol is predicted to be 8.21 eV. To facilitate the interpretation, we grouped them by the type of $-OCH_3$ conformation (*trans*, *gauche*, *all-gauche*) and the orientation of CH_3OH (*in*, *out*). The populations, averaged relative energies, and averaged VIEs are shown in Figure 4.

For the neutral molecule, the two clearly dominant conformer types are *trans-in* and *gauche-in*. For the correspond-

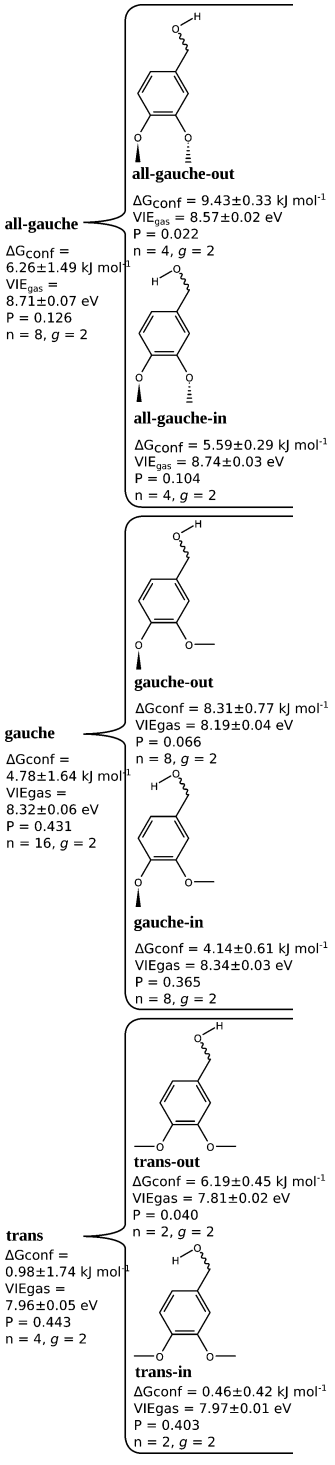

Figure 4. Stable gas phase conformers of veratrole alcohol. Populations *P* are derived from Boltzmann statistics at T = 298 K, n is the total number of unique conformers in one group, and g is their degeneracy. Relative free energies (with respect to the lowest energy conformer) and VIE_{gas} numbers are weighted averages over different conformers, obtained from ROCBSQB3 calculations. Listed distribution widths are weighted standard deviations.

dx.doi.org/10.1021/jp508053m | J. Phys. Chem. B 2015, 119, 238−256

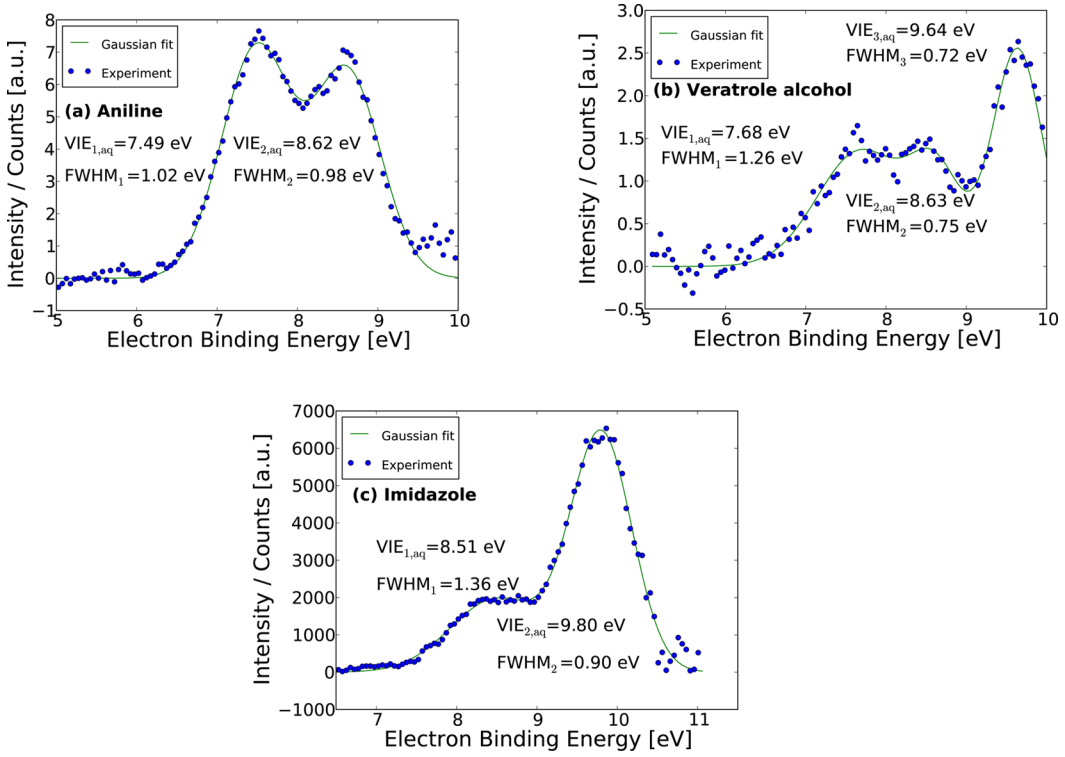

Figure 5. Aqueous phase photoelectron spectra of (a) aniline, (b) veratrole alcohol, and (c) imidazole. Peak positions (VIE) and full widths at half-maximum (FWHM) from Gaussian fits are shown in the panels.

ing cation, *trans-out* conformations were found to be the only stable structures. Using VIE data of the neutral state as a proxy to gain insight into ionized state energetics, we estimate that the unstable *gauche* conformations would lie ≈40 kJ mol^{-1} to 50 kJ mol^{-1} higher than those of the *trans* conformers.

Summary of Gas Phase Ionization Energy Results. Our modified ROCBSQB3 and W1 protocols were found to predict AIE$_{gas}$ of rigid organic molecules to within 0.04 and 0.08 eV, respectively. For VIE$_{gas}$, computed W1 and ROCBSQB3 values fall within 0.04 eV of the ranges of published values, with the exception of DMS, for which the discrepancy amounts to 0.1 eV. Given the good performance of these computational methods for AIE$_{gas}$, we prefer the use of computed VIE$_{gas}$ values for the analysis of solvation effects, as these do not suffer from apparently substantial experimental uncertainties. Additionally, based on the observed good quality of CBSQB3 computed ionization energies, we use this method to estimate AIE$_{gas}$ and VIE$_{gas}$ values where no experimental data are available. This included the adiabatic and vertical ionization energies of veratrole alcohol and thymidine. For these two compounds, the (RO−)CBSQB3 method works well for their smaller analogues, ODMB and thymine.

Uncertainties in computed VIE$_{gas}$ values may arise in molecules with significant conformational freedom. For ODMB, the shapes of the potential energy surfaces are very different in the reduced and oxidized state, and thus the VIE$_{gas}$ values of different neutral conformers can be quite different from each other. Consequently, small errors in the population analysis can lead to large errors in the predicted mean VIE$_{gas}$. Nevertheless, we obtained good agreement between computation and experiment for relative populations of ODMB conformers, as well as corresponding AIE$_{gas}$ and VIE$_{gas}$ values. Thus, we expect reasonable results for our reported predictions for the structural analogue veratrole alcohol.

Finally, we did not perform an extensive conformational search for thymidine. For this flexible system, many stable gas phase conformers exist,[88] several of which are close in energy. An accurate evaluation of conformer populations for a molecule of this size would be expensive, and a detailed study of the influence of thymidine conformations on the gas phase VIEs was beyond the scope of the present study. The data in the present manuscript is based on a single conformer that does not exhibit an intramolecular H-bond from the sugar to thymine, in analogy to a previous study on the photoelectron spectra of thymidine.[26] H-bonding to the thymine unit is expected to raise the VIE (see Figure 10 and related discussion), and the VIE$_{gas}$ reported here represents a lower bound. Considering the proximity in energy of conformations with and without intramolecular H-bond,[88] the true VIE$_{gas}$ may be as much as ≈0.15 eV higher in energy than the 8.74 eV reported in Table 1. (For comparison, another single-conformer VIE$_{gas}$ of thymidine was previously estimated to be 8.58 eV with a different methodology.[26]) The AIE$_{gas}$ should be less affected, for reasons analogous to veratrole alcohol. In the oxidized state, we expect conformers exhibiting an intramolecular hydrogen bond to be high in energy, and thus to either not be stable minima or to remain unpopulated. Thus, our best estimate for VIE$_{gas}$ of thymidine is 8.7 to 8.9 eV, and this uncertainty propagates to λ_{gas} and ΔVIE$_{aq}$ (see below). Owing to the interest in thymidine ionization from a biological point of view, the influence of conformers on the VIEs of thymidine warrant further studies.

Aqueous Photoelectron Spectroscopy. We measured liquid aqueous microjet PE spectra of aniline, veratrole alcohol, imidazole, and methoxybenzene. For the first three of these compounds, the lowest aqueous VIE$_{aq}$ values can be extracted from PES data. From available experimental VIE$_{aq}$ data and our computed VIE$_{gas}$ data, we can determine ΔVIE$_{aq}$ values. For

dx.doi.org/10.1021/jp508053m | J. Phys. Chem. B 2015, 119, 238−256

Table 2. Best Estimates of Gas Phase and Solution Phase Ionization Properties of Selected Molecules (eV)

	aniline	phenol	veratrole alcohol	phenolate	imidazole	thymidine[h]	imidazolium	DMS	methoxybenzene
					gas phase energies				
$VIE_{gas,298K}$[a]	8.04	8.75	8.21[b]	2.31	9.11	8.7−8.9	15.30	8.81	8.47
$AIE_{gas,298K}$[c]	7.73	8.52	7.48	2.24	8.82	8.3	15.04	8.65	8.23
$\lambda_{gas,298K}$	0.31	0.23	0.73	0.08	0.29	0.5−0.6	0.25	0.16	0.23
					aqueous phase energies				
$VIE_{aq,298K}$[d]	7.49	7.84	7.68	7.10	8.51	8.30	8.96	8.26[e]	8.09[e]
$AIE_{aq,298K}$[f]	5.27	5.75	5.61	5.04				5.91	5.87
$\lambda_{aq,298K}$	2.22	2.09	2.07	2.06				2.35[e]	2.22[e]
					differences between aqueous and gas phase				
ΔVIE_{aq}	−0.55	−0.91	−0.53	4.79	−0.60	(0.4−0.6)	−6.34		
$\Delta VIE_{aq,comp}$	−0.77	−0.65	(−0.54)[g]		−0.67			−0.54	−0.39
ΔAIE_{aq}	−2.46	−2.77	−1.87	2.80				−2.75	−2.36
$\Delta\lambda_{aq}$	1.91	1.86	1.34	1.99				2.21[e]	1.99[e]

[a]Best computational estimate. W1BD for aniline, phenol, imidazole, imidazolium; ROCBSQB3 for veratrole alcohol and thymidine. [b]VIE_{gas} for veratrole alcohol is a weighted average based on computed conformer populations. [c]For consistency, values computed with the same level of theory as VIE_{gas} are used instead of experimental values. Calculated from data in Table 1 as $AIE_{gas,298K} = AIE_{gas,0K} - \Delta E_{ZPVE} + \Delta G_{rotvib}$, except for veratrole alcohol (see text). [d]Aqueous microjet PE values from this work, as well as literature data[26,27] for phenol, phenolate, and imidazolium. [e]These values are based on MD simulations of the VIE_{aq}. [f]Determined from literature values of oxidation potentials[91−96] using eq 1. [g]Considering data exclusively for the *gauche* conformer, which is likely the most abundant conformer in both gas and aqueous phase. [h]Gas phase data computed on a single conformer, which may represent an underestimate of the conformer-averaged VIE_{gas}. See text for details.

aniline and veratrole alcohol, experimental aqueous oxidation potentials are also available, which allows the determination of half-cell aqueous reorganization energies (λ_{aq}) for these compounds.

Experimental Aqueous Phase Photoelectron Spectra. Measured aqueous PE spectra (Figure 5) reveal two well-defined VIE_{aq} bands at 7.49 and 8.62 eV for aniline and three VIE_{aq} bands at 7.68, 8.63, and 9.64 eV for veratrole alcohol. Each successive band corresponds to the ejection of single electrons of increasing binding energy from the solvated molecule. We also report an updated photoelectron spectrum of imidazole, which features two distinct bands at 8.51 and 9.80 eV. The lowest band, VIE_{aq}, differs significantly from the previously reported value of 8.26 eV.[24] The current imidazole measurement improves over the old one: it features a better signal-to-noise ratio, the addition of salt to the solution to counter charging effects, and likely a lower gas-phase contribution to the signal. For methoxybenzene, the measured signal is too weak to allow a reliable quantitative determination of VIE_{aq}, presumably owing to the lower solubility of this compound (Figure S1). Finally, to enable further data comparisons including previously unreported peak widths, we also analyzed published aqueous microjet PES data for phenol,[27] for which we refitted VIE_{aq} and $VIE_{2,aq}$ values of 7.84 and 8.68 eV. These values agree with the previously reported peak positions of 7.8 ± 0.1 eV and 8.6 ± 0.1 eV, respectively.

For the neutral species aniline, imidazole, veratrole alcohol, thymidine, and phenol, the measured VIE_{aq} value is substantially red-shifted with respect to the computed VIE_{gas} value, indicating that aqueous solvent stabilizes the vertical ionization. For these compounds, ΔVIE_{aq} values range from ≈−0.5 to −0.91 eV (Table 2). By comparison, the positively charged imidazolium exhibits a much larger ΔVIE_{aq} value of −6.34 eV. This suggests that a beneficial orientation of solvent dipoles, already organized by the reduced monovalent cation, enables the divalent cationic oxidized species to receive substantial stabilization by the solvent. Conversely, the presence of solvent is severely destabilizing for the VIE of phenolate, which exhibits a highly unfavorable ΔVIE_{aq} value of 4.79 eV. This can be explained by the organized orientation of solvent dipoles around the anionic reduced solute, an arrangement that is apparently highly destabilized in the oxidized neutral state.

Aqueous PE spectral bands are significantly broadened compared to the same features in the gas phase spectra. For aniline, we fitted $FWHM_{1,aq}$ = 1.02 eV and $FWHM_{2,aq}$ = 0.98 eV, whereas gas phase spectra produce $FWHM_{1,gas}$ = 0.6 eV, and $FWHM_{2,gas}$ = 0.4 eV.[84] Similarly, for phenol we obtained $FWHM_{1,aq}$ = 1.10 eV and $FWHM_{2,aq}$ = 0.84 eV, whereas the extracted gas phase values[84] are 0.5 and 0.4 eV, respectively. Peak broadening in the aqueous phase arises because different solvent conformations lead to increased variability in the stabilization of both the reduced and oxidized states.

Although PE spectral bands are red-shifted by the presence of aqueous solvent, we observe that interpeak distances remain unchanged in aqueous phase spectra relative to gas phase spectra. For aniline, the interpeak distance of the two lowest bands in the aqueous PES is ≈1.1 eV, which is similar to the gas phase interpeak distance of ≈1.1 eV.[84] For imidazole, the lowest two bands exhibit an interpeak distance of 1.29 eV in both aqueous phase (this study) and gas phase.[76,89] For phenol, the interpeak distance VIE_1 and VIE_2 changes by 0.1 eV upon solvation, when compared to the gas phase spectrum.[84] These results suggest that the solvent-induced stabilization is of similar magnitude for the different pairs of valence electrons and associated vertically ionized states, rationalized as follows. For the small aromatic systems considered here (aniline, phenol, imidazole), the orbitals involved in the lowest transitions are delocalized π-orbitals of the aromatic ring. This is supported by gas phase EOM-IP-CCSD calculations, which identified ionization from delocalized π-orbitals of the Hartree−Fock reference as the main contributions to both VIE_{gas} and $VIE_{2,gas}$. Owing to the delocalized nature of the resulting electron hole,

dx.doi.org/10.1021/jp508053m | J. Phys. Chem. B 2015, 119, 238−256

the electrostatic potentials of the first and second vertically ionized states may indeed be similar. As a result, the electrostatic interactions between the solvent and the different lowest electronic states of the radical cation could be of similar magnitude, resulting in the observed conservation of the interpeak distance in solution relative to gas phase.

Finally, insight into the aqueous PE spectrum of veratrole alcohol is less clear. Our analysis of gas phase PE spectra for ODMB and simulations of the gas phase spectrum of veratrole alcohol revealed that different conformers can have varying VIE_{gas} values (above). Hence, theoretical simulations are needed to guide further interpretation of the aqueous PE spectrum data of this flexible molecule, as is shown below.

Reorganization Energies in Gas and Aqueous Phase. With the aim of better understanding the role of solvent reorganization in one-electron oxidation reactions, we extended the available database (phenol, phenolate)[27] of half-cell aqueous reorganization energies, λ_{aq}, to include aniline and veratrole alcohol. λ_{aq} can be deduced from experimental data by subtracting the AIE_{aq} from the VIE_{aq} (eq 1). This definition of λ_{aq} is not restricted by the LRA employed in Marcus theory.[19,29,30] We used literature values of oxidation potentials and measured VIE_{aq} data to determine λ_{aq} (Table 2).

In analogy to inner- and outer-sphere reorganization energies in Marcus theory, λ_i and λ_o, we can additionally separate λ_{aq} of the half-cell reaction into gas phase and solvation contributions,[90] where $\lambda_{aq} = \lambda_{gas} + \Delta\lambda_{aq}$ (Table 2 and Figure 6). We

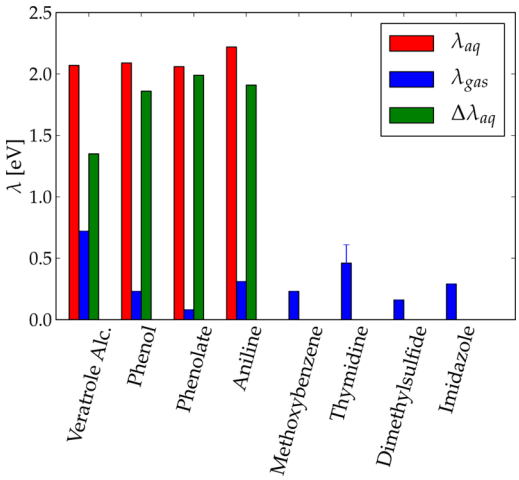

Figure 6. Reorganization energies λ_{aq} of different organic molecules, apportioned into a gas phase component (λ_{gas}) and a contribution from solvation effects ($\Delta\lambda_{aq}$).

determined λ_{gas} values based on the best available gas phase quantum chemical calculation results (Table 2). λ_{gas} values of neutral molecules vary between 0.14 eV (dimethylsulfide) and 0.73 eV (veratrole alcohol). Experimental λ_{aq} values exhibit surprising constancy, ranging from 2.06 to 2.22 eV for aniline, phenol, veratrole alcohol, and phenolate, about an order of magnitude larger than gas phase values.

Inspection of λ_{aq}, $\Delta\lambda_{aq}$, and λ_{gas} data raise questions about the origins of contributions to the reorganization energy in solution (Table 2, Figure 6). For aniline, λ_{gas}, linked to planarization of the amino group in addition to structural changes in the ring, is 0.08 eV higher than the value for phenol. Together with an additionally higher $\Delta\lambda_{aq}$ value (0.05 eV), aniline thus yields a somewhat higher λ_{aq} value than phenol. For veratrole alcohol, the designation of a λ_{gas} value is more difficult, due to the uncertainties in the computed conformer populations. Moreover, the experimental λ_{aq} value of veratrole alcohol should contain changes in the conformer population when going from the vertically ionized state to the relaxed ionized state. In contrast to the gas phase, in aqueous solvation, we expect the *gauche-out* and *trans-out* conformers to be dominant for the reduced species, and *trans-out* to be the only dominant conformation for the oxidized species. Compared to the gas phase, an additional increase in λ due to *in* conformers is missing. We recalculated λ_{gas} considering only the *out* conformers, leading to VIE_{gas} =8.14 eV and AIE_{gas} =7.43 eV. Based on these data, $\lambda_{gas,\,out}$ remains high at 0.71 eV. Hence, we would expect this gas phase contribution to propagate to λ_{aq}, and it remained unclear why this is not the case. These λ_{aq} and $\Delta\lambda_{aq}$ data are not easily interpretable and warrant further computational studies that include the calculation of oxidation potentials.

Simulated Aqueous PE Spectra by Ab Initio Molecular Dynamics. For aniline, phenol, imidazole, veratrole alcohol, methoxybenzene, and DMS, we simulated complete photoelectron spectra comprised of the two or three lowest aqueous vertical ionization energy bands. This was achieved by performing quantum mechanics/molecular mechanics (QM/MM) molecular dynamics (MD) simulations of each organic solute (QM) in a bath of water molecules (MM), using periodic boundary conditions. We calculated valence VIE_{aq}, $VIE_{2,aq}$, and $VIE_{3,aq}$ values on 499 clusters ("snapshots") extracted from each production MD trajectory, where each cluster included the solute (described with EOM-IP-CCSD) and the 3072 water molecules (described with effective fragment potentials) most proximate to the solute. Calculations with several additional cluster sizes, centered on the solute, were performed to ensure the convergence of the VIE distribution with respect to cluster size.

Convergence of the Simulated VIE_{aq}. We ensured that our simulated VIE_{aq} values were converged in two ways: (a) the convergence of the averaged ionization energy with respect to simulation time and number of considered snapshots, and (b) the convergence of the averaged ionization energy with respect to the number of water molecules included in the solvent cluster. For aniline, phenol, imidazole, methoxybenzene, and DMS, the averaged VIE_{aq} stabilizes to within $\pm$0.02 eV after 25 ps of simulation time (Figure S2). In Figure 7b, we show the convergence of the average VIE_{aq} as well as the Gaussian-fitted VIE_{aq} with respect to the effective radius of the simulated solute−solvent cluster. Beyond ≈256 water molecules, there are only small changes of the VIE distribution, and the distributions obtained with 2048 or more water molecules are barely distinguishable from each other. We consider the averaged VIE values to be sufficiently converged at an effective cluster radius of ≈25 Å, corresponding to a cluster containing the 3072 water molecules most proximate to the solute. At this cluster size, the shape of the VIE distribution has stabilized as well (Figure 7a). The simulation VIE_{aq} data reported in Figure S2 and in the remainder of the article are based on solvent clusters containing 3072 water molecules.

Owing to the computational cost, detailed convergence studies as shown in Figure 7 were only performed for imidazole. We performed computations up to the first 32 water molecules for the other organics as well, which exhibited significant differences in ΔVIE, attributable to difference in water orientation close to the solute. However, we expect the

dx.doi.org/10.1021/jp508053m | J. Phys. Chem. B 2015, 119, 238−256

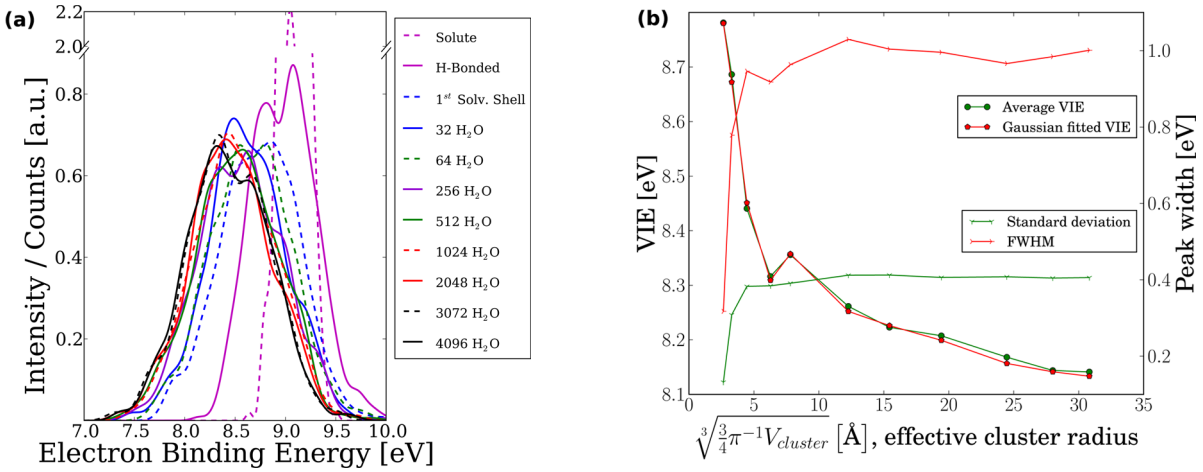

Figure 7. Convergence of the distribution of the simulated first spectral band of imidazole (499 snapshots) with increasing size of the water cluster used. (a) Evolution of the simulated spectral band with increasing cluster size. (b) Evolution of the averaged VIE and Gaussian-fitted VIE (left axis) and evolution of the peak width, described as standard deviation and full width at half-maximum (FWHM) (right axis), for the spectral band shown in (a), plotted vs the cube root of the cluster volume.

long-range convergence of the VIE with solvent cluster size to be comparable for the singly charged organics studied here: in all cases, the charge is delocalized in a single aromatic ring. Slightly larger cluster volumes could be necessary in special cases like strongly delocalized, nonspherical charge distributions, and further testing is advised in exotic cases.

Comparison of Simulated and Experimental Aqueous PE Spectra. Good agreement was found between simulated and experimental aqueous PE spectra for aniline, veratrole alcohol, phenol, and imidazole (Figure 8). Simulated peak positions of the VIE_{aq} match experiment to within 0.26 eV or less for all four compounds. Experimental peak widths range from 0.75 to 1.36 eV, expressed as FWHM values. By comparison, simulated peak widths are 1.00 ± 0.05 eV. Thus, the experimental peak positions, peak widths, and peak shapes are generally well-reproduced by simulation for all of these compounds. The simulated ΔVIE_{aq} of phenol, −0.65 eV, is in excellent agreement with the value of −0.66 eV obtained in a previous study[27] in which a similar computational protocol was used. Computed ΔVIE_{aq} values are summarized in Table 2.

For methoxybenzene, where the experimental signal is weak, only modest agreement between simulation and experiment was achieved. Possible sources for this discrepancy may be (i) insufficient experimental signal to enable meaningful interpretation; (ii) a weaker peak intensity of VIE_{aq} relative to the $VIE_{2,aq}$ band, an effect not considered during the simulation (see below); and (iii) accumulation of the solute at the air−water interface, leading to gas-like contributions to the measured aqueous spectrum (VIE_{gas} is estimated to be 8.47 eV, Table 2).

A phenomenon we did not address is that of relative peak intensities. For example, the aqueous PE spectrum of imidazole features a $VIE_{2,aq}$ peak of higher intensity than the VIE_{aq} peak. This trend is also observed in the gas phase spectrum.[76] For aniline, the aqueous phase VIE_{aq} peak is slightly more intense than $VIE_{2,aq}$, whereas in the gas phase this trend is reversed. Veratrole alcohol exhibits a substantially increased peak intensity for $VIE_{3,aq}$ compared to VIE_{aq} and $VIE_{2,aq}$, but this trend is not observed in the gas phase PE spectrum of the analogue ODMB. These observed changes in relative peak intensities may result from both solvation effects and from the anisotropy parameter[97] that governs the differential photoionization cross sections in solution. Appropriate protocols[98,99] should be applied to solvated calculations directly to further explore these effects.

Origins of the ΔVIE_{aq}. How can we further explore the effects of solvation on the vertical ionization process? To gain additional insight into this phenomenon, we conducted additional analysis on the shift in the vertical ionization energy upon going from gas phase into solution, ΔVIE_{aq} (eq 2). For aniline, imidazole, and phenol, the experimental and simulated ΔVIE_{aq} values agree to within 0.26 eV (Table 2, Figure 9). For veratrole alcohol, the experimental value of ΔVIE_{aq} is calculated using the VIE_{gas} value based on computed conformer weights, described above. This averaged VIE_{gas} value was subtracted from the (bulk) experimental VIE_{aq}. As the BLYP-D2-based dihedral angle distribution of the veratrole alcohol MD simulation is biased and not well-converged (Figure S3), we do not provide a computed ΔVIE_{aq} value. However, as the computed VIE_{aq} of individual regions of dihedral angle space were found to be well-converged (see below), we provide this decomposition for different conformer groups.

Based on simulation data, we decomposed the ΔVIE_{aq} into two separate contributions. We consider the change in VIE arising from the deformation of the solute due to solvation, ΔVIE_{def}, as

$$\Delta VIE_{def} = VIE_{0\text{-}H_2O} - VIE_{gas} \quad (13)$$

where $VIE_{0\text{-}H_2O}$ represents the VIE computed in gas phase, using the ensemble of solute geometries extracted from the aqueous MD simulation. VIE_{gas} is computed on the stationary gas phase structure. The second energy component describes the change in VIE arising from hydration of the deformed solute structure, ΔVIE_{hydr}, defined as

$$\Delta VIE_{hydr} = VIE_{3072\text{-}H_2O} - VIE_{0\text{-}H_2O} \quad (14)$$

where $VIE_{3072\text{-}H_2O}$ corresponds to the fully hydrated system that was used to compute ΔVIE_{aq}. Consequently ΔVIE_{aq} is partitioned as follows:

$$\Delta VIE_{aq} = \Delta VIE_{def} + \Delta VIE_{hydr} \quad (15)$$

dx.doi.org/10.1021/jp508053m | J. Phys. Chem. B 2015, 119, 238−256

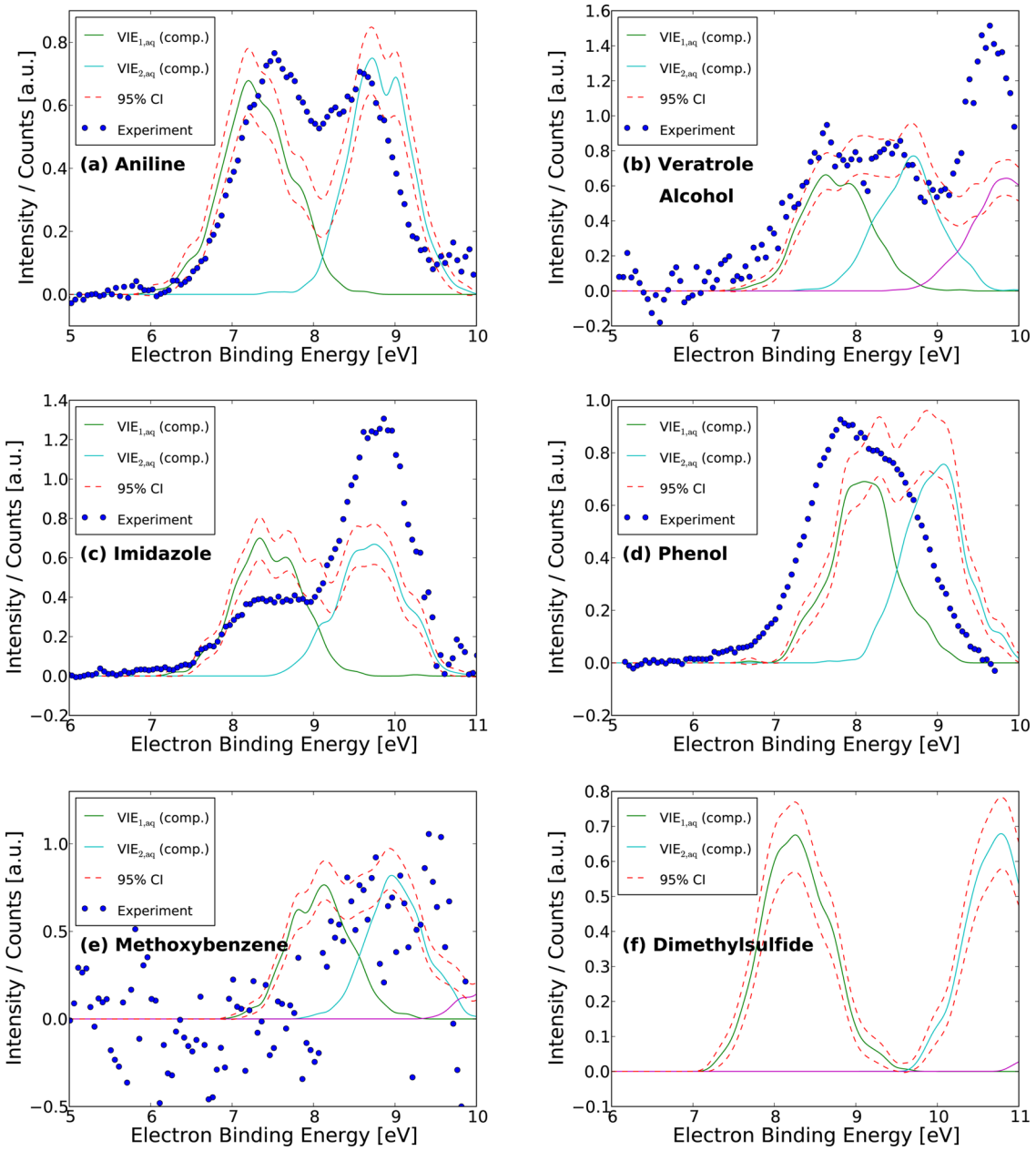

Figure 8. Comparisons between simulated spectra (solid lines) and experimental VIE_{aq} spectra (circles), accounting for the first two or three ionizations. The red dashed lines envelop the 95% confidence interval (CI) of the simulated spectrum, indicating the uncertainty due to finite sample size.

The magnitude of these contributions to ΔVIE_{aq} are shown for six different solutes in Figure 9.

For all studied compounds, ΔVIE_{hydr} is large and negative (−0.35 to −0.72 eV), corresponding to a lowering of the VIE upon hydration. The ΔVIE_{hydr} is larger, on average, for the compounds that contain hydrogen bond donor moieties (phenol, aniline, imidazole) compared to those that do not (methoxybenzene, DMS). This is consistent with the observations of Ghosh et al. who simulated VIE values for microsolvated clusters of phenol[27] and thymine.[100] Ghosh and co-workers found that water molecules acting as H-bond donors increase the cluster VIE, whereas water molecules acting as H-bond acceptors decreased the VIE. To explore these trends further, we performed additional calculations on gas-phase solute−water clusters using several different solutes, including phenolate, methoxybenzene, veratrole alcohol, thymidine, aniline, phenol, imidazole, and imidazolium. From simulations of these small clusters, we found that water molecules acting as H-bond donor always increase the VIE, whereas water molecules acting as H-bond acceptors always decrease the VIE (Figure 10). Thus, several lines of evidence indicate that solute H-bond donor groups contribute to an increase of the ΔVIE_{aq}, whereas solute H-bond acceptor groups contribute to a lowering of the ΔVIE_{aq}. A proposed explanation for this behavior is provided in the Supporting Information (SI).

Water molecules more distant from the ionized solute should lower the VIE_{aq} irrespective of their orientations, on average, through polarization of their electron density. This is illustrated by the evolution of ΔVIE with increasing cluster size in Figure

dx.doi.org/10.1021/jp508053m | J. Phys. Chem. B 2015, 119, 238−256

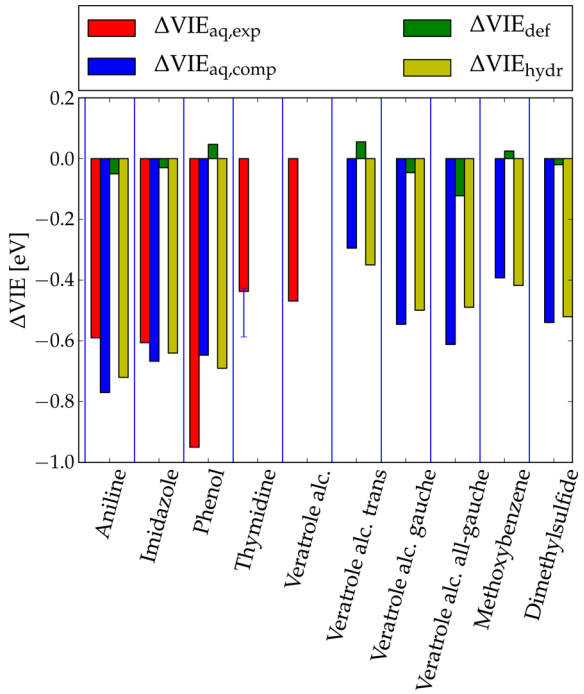

Figure 9. Experimental and computed ΔVIE_{aq} values for different compounds, and the different contributions arising from solute deformation (ΔVIE_{def}) and hydration (ΔVIE_{hydr}). Value using weighted conformer average for the gas phase and the plain MD-based VIE_{aq}.

7. These data are again in qualitative agreement with Ghosh et al.,[100] who evaluated the trend in VIE with respect to the length of a static chain of water molecules extending away from the solute. They found that the VIE stabilizes at a radial chain length of ≈25 Å, which is in good agreement with the convergence of the fully hydrated ΔVIE_{aq} that we report in Figure 7.

The change in ΔVIE_{aq} attributable to solute deformation, ΔVIE_{def}, is small for all compounds that we studied, having an absolute magnitude of ≤0.06 eV for all cases except the *all-gauche* conformer of veratrole alcohol. In the cases where ΔVIE_{def} is positive (phenol, methoxybenzene, and veratrole alcohol *trans* conformers), this increase in VIE can be ascribed to out-of-plane bending of either the OCH_3 or OH substituents during the MD simulations. Compared to the planar stationary structures of these molecules, the stabilization of the oxidized radical cation through positive mesomeric effects is less pronounced in the out-of-plane deformed structures.

In veratrole alcohol, two antagonistic effects act on ΔVIE_{def}: On one hand, the *in* conformers of the $-CH_2OH$ group are not populated in solution, as H-bonding to solvent out-competes the OH-π interaction dominant in the gas phase. This results in a negative contribution to ΔVIE_{def} for all types of conformers (*trans*, *gauche*, *all-gauche*) of ≈−0.1 eV. On the other hand, the "planar" $-OCH_3$ groups of the *trans* and *gauche* conformers deplanarize during the MD simulation: we consider only the stationary, planar structure in the gas phase, whereas in the aqueous MD simulations, all geometries with dihedral angles of the methoxy groups <70° were defined as *trans* (see below). Owing to the flat torsional potential of *o*-methoxy groups, the gas phase system is also expected to explore dihedral angles significantly different from zero but within the basin centered around the planar *trans* conformation. This deplanarization adds a positive contribution to the ΔVIE_{def} values of the individual conformers, balancing the negative contribution of the absence of *in* conformers. For the *all-gauche* conformer, however, further deplanarization is not possible, hence, the larger negative ΔVIE_{def} of −0.12 eV.

Role of Conformational Dynamics for Aqueous Vertical Ionization of Veratrole Alcohol. The facile rotation of the *o*-methoxy groups of veratrole alcohol in aqueous solution at 298 K allowed us to explore the influence of solute conformational dynamics on the VIE_{aq}. This feature does not arise for most of the other molecules considered in this study. Analysis of the veratrole alcohol MD trajectory reveals that the planar and *gauche* conformations are equally populated (51:49%). In analogy to the gas phase, the VIE_{aq} is higher for the out-of-plane conformers, although this effect is found to be screened by hydration effects.

Previous studies have explored the conformations of the structural analogue ODMB in different organic solvents. Authors have reported the solvent dependence of planarity

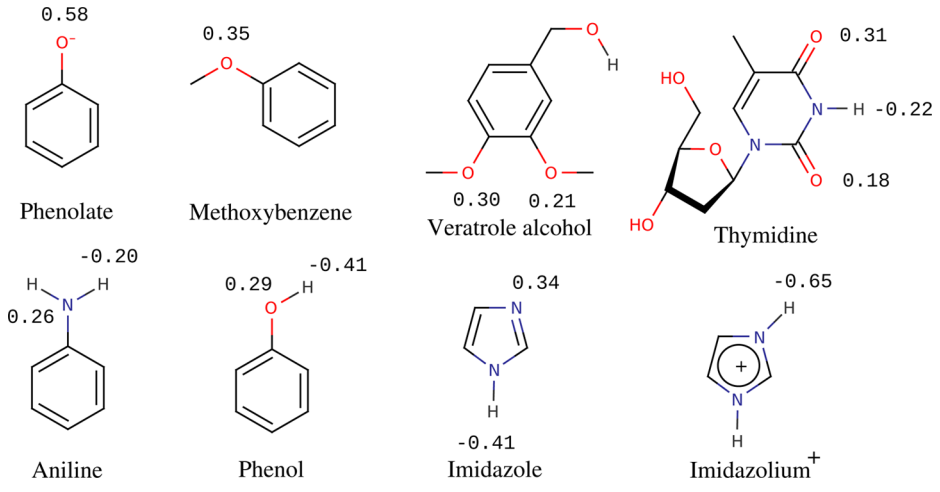

Figure 10. Computed $\Delta VIE_{1\cdot H_2O}$ values for different compounds (eV), computed with the (RO)BHandHLYP/aug-cc-pVTZ//M06L/aug-cc-pVDZ model chemistry. Each $\Delta VIE_{1\cdot H_2O}$ value is printed next to the H-bond donating or accepting site to which the explicit water molecule is associated. The two listed values for veratrole alcohol correspond to two different water orientations.

dx.doi.org/10.1021/jp508053m | J. Phys. Chem. B 2015, 119, 238−256

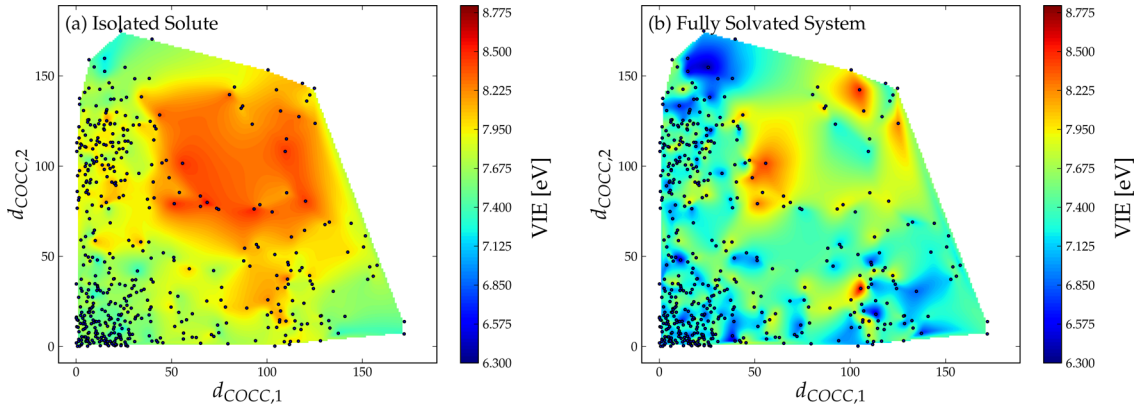

Figure 11. Heat maps of the first VIE of veratrole alcohol as a function of the dihedral angles $d_{COCC,1}$ and $d_{COCC,2}$ of both methoxy groups relative to the aromatic ring. (a) VIE_{gas} values were evaluated on unsolvated geometries of the solute taken from snapshots of aqueous MD simulations; (b) VIE_{aq} values taken from snapshots of aqueous MD simulations. High values are shaded red and low values are shaded blue. The positions of individual snapshot VIE values are indicated as black dots.

versus nonplanarity of ODMB in low-temperature glasses[101] and in the liquid phase.[101−104] However, the experimental reports leave it unclear whether nonplanarity implies only a temporary departure from planarity within the basin centered at the planar minimum, or whether, like in the gas phase, stable nonplanar conformers exist. To the best of our knowledge, there are no published data for the conformer populations of ODMB in the aqueous phase. We aimed to clarify whether nonplanar structures are visited in aqueous solution and, if so, whether these nonplanar structures represent stable conformers. Owing to the structural similarity between ODMB and veratrole alcohol, we assume that the conformational structures of these two molecules should be similar in any solvent, and that the results presented below for veratrole alcohol would be transferable to an aqueous solution of ODMB.

Does a stable *gauche* conformer exist for veratrole alcohol in aqueous solution? Based on the observation that the gas-phase barrier of the out-of-plane torsion is at about 70°, we divided the conformational space of aqueous simulations into two regions: one viewed as "planar" conformation (d_{COCC} < 70°) and the other as "nonplanar" (d_{COCC} > 70°) conformation. In Figure 11b, we show the visitation of aqueous phase conformers in the space spanned by the two COCC dihedral angles, based on MD simulations. According to MD simulations, these two regions are populated equally (51:49%), consistent with the interpretation that these two conformers exhibit a very low free energy difference in solution. Notably, the regions that lie in close proximity to the gas phase stationary structures, $d_{COCC,1/2}$ = 0° and $d_{COCC,1/2}$ = 110°, are more densely populated compared to the regions corresponding to the gas phase transition structures ($d_{COCC,1/2}$ = 70°). This indicates that two stable basins, separated by a barrier, exist in aqueous simulations. This interpretation is further supported by the observed evolution of the dihedral angles with time (Figure 11b). The aqueous solvated system spends extended periods of time (≈1 to 5 ps) in the nonplanar (*gauche*) conformations, whereas the observed switches between the *trans* and *gauche* regions are much more rapid, occurring on time frames of 0.2 to 0.5 ps.

Is the *gauche* conformer of veratrole alcohol stabilized in aqueous phase with respect to the gas phase? This question is more difficult to answer, owing to technical shortcomings of the methods used in the simulation. The model chemistry employed in the QM/MM molecular dynamics simulation, BLYP-D2/TZVPP, overestimates the relative gas phase energy of the *gauche* conformer by ≈4 kJ mol^{-1}. Thus, BLYP-D2/TZVPP would predict the *trans* conformer to be the uncontroversially dominant species in gas phase. However, this is clearly not the case, based on our analysis of ODMB and veratrole alcohol conformers with accurate thermochemical protocols (see above). As a consequence, gas phase BLYP-D2 MD results (Figure S3a) leave the *gauche* conformer unpopulated, whereas the real population should be ≈50%. However, aqueous BLYP-D2 MD simulations predict that the gauche basins are significantly populated (≈50%), indicating that the energy of this basin is lowered with respect to the gas phase. Thus, BLYP-D2 simulations suggest that the gauche conformer is indeed stabilized in aqueous solution relative to the gas phase. Nonetheless, this inference should be extended only tentatively to the real system, since the BLYP-D2/TZVPP model chemistry has unclear reliability for this subtle energy difference.

Finally, what is the influence of the methoxy group d_{COCC} dihedral angle on the VIE_{aq} of veratrole alcohol? Before discussing the effect of aqueous solvation, we consider the influence of the two methoxy group dihedral angles on the VIE_{gas} evaluated with unsolvated geometries extracted from aqueous MD simulations (Figure 11a). The trends observed for veratrole alcohol are comparable to the gas phase results found with partly constrained geometries of ODMB (Figure 3), where nonplanarity leads to an increase in VIE_{gas}. This can be rationalized by resonance arguments: the positive mesomeric effect of the methoxy groups is much more pronounced in the ionized species, creating a second minimum at the *cis* conformer, which is a transition state for the neutral compound. The behavior of veratrole alcohol $VIE_{2,gas}$ and $VIE_{3,gas}$ values (evaluated on desolvated geometries from aqueous MD simulations) is also comparable to the corresponding gas phase results found with partly constrained geometries of ODMB (Figure 3). Aqueous solvation masks this clear relationship between d_{COCC} and VIE (Figure 11b), although the overall increase of VIE_{aq} with nonplanarity is still present. The averaged difference between the surfaces shown in Figure 11a,b amounts to ΔVIE_{hydr} (Figure 9). Partitioning the stable conformers as described above, we find that ΔVIE_{hydr} is more negative for the *gauche* conformer compared to the *trans* conformer. This offsets the higher intrinsic VIE_{gas} value of the

dx.doi.org/10.1021/jp508053m | J. Phys. Chem. B 2015, 119, 238−256

gauche conformer, explaining why the computed VIE_{aq} values of the *gauche* and *trans* conformers are separated by only 0.1 eV. Thus, both of these conformers occupy the lowest VIE_{aq} band in the aqueous PE spectrum (Figure 5). This illustrates clearly that the experimental PE spectra of flexible molecules may be difficult or impossible to interpret without the support of theoretical calculations.

CONCLUSIONS

In this study we present simulation data describing the aqueous vertical ionization process for six organic molecules, including aniline, imidazole, veratrole alcohol, methoxybenzene, phenol, and dimethylsulfide. New liquid microjet aqueous PE spectrum data are presented for the first four of these compounds. Using a fully solvated QM/MM protocol to generate a molecular dynamics trajectory and employing EOM-IP-CCSD with EFPs to describe the vertical ionization of solvent clusters, we correctly reproduce the positions (±0.26 eV) and widths (±0.3 eV) of the lowest two to three valence vertical ionization bands of four molecules for which reasonably resolved experimental data are available.

Experimental and simulation data enable us to investigate the physical nature of the VIE_{aq}. We decompose VIE_{aq} into a gas phase component, VIE_{gas}, and a component describing the effect of aqueous solution, ΔVIE_{aq}, for each solute. For six neutral organic molecules (aniline, veratrole alcohol, imidazole, thymidine, phenol, and DMS), we find that aqueous solution stabilizes the first vertical ionization energy by ≈−0.5 to −0.91 eV, compared to the gas phase.

With the aid of simulations, we further investigate the influence of aqueous solvent on the VIE. We partition the ΔVIE_{aq} into the influence of deforming the gas phase solute into its conformation in solution, ΔVIE_{def}, and a component describing the influence of hydration of the solute, ΔVIE_{hydr}. We find that solute H-bond acceptor groups lead to an increase in the ΔVIE_{hydr}, and solute H-bond donor groups lead to a decrease in the ΔVIE_{hydr}. These trends are consistent with earlier observations of Ghosh and co-workers.[27,100] It remains unclear whether phenol, which is amphoteric, obeys these trends. Phenol displays a large and negative ΔVIE_{aq} value, despite being a good H-bond donor. Phenol also exhibits the largest discrepancy between computed and experimental ΔVIE_{aq} values. Hence, the interplay between solvation pattern and ΔVIE_{aq} is yet to be fully understood. To investigate this phenomenon in more detail, it would be informative to evaluate ΔVIE_{aq} for other compounds that contain aromatic −OH functionalities, for example, benzenediols, as well as other chemical families not considered in this study.

In-depth analysis of the aqueous vertical ionization of a flexible molecule, veratrole alcohol, is revealing. Simulation data indicate that multiple stable conformers of veratrole alcohol exist in gas phase and also in aqueous solution. Individual conformers are found to exhibit distinct VIE values, both in the gas phase and in solution, due to the dependence of the VIE on the dihedral angles of the two methoxy groups of the phenyl ring. This provides direct evidence that electron transfers in solution are likely to be conformation-dependent for flexible molecules. These results also illustrate that the interpretation of experimental PE spectra may be complicated by the possible existence of multiple stable conformers. Similar situations likely exist for thymidine and other flexible molecules, owing to the large differences of the reduced and oxidized potential energy surfaces. Future investigations of such systems will be valuably aided by molecular simulations.

VIE_{aq} data can be used to estimate one-electron reorganization energies of the donor half-cell reaction, in cases where the oxidation potential is also known. A surprising result is the apparent constancy of λ_{aq} among the six compounds for which we could determine or estimate this property. This implies that in outer sphere electron transfer reactions involving different organic reductants, the λ_{aq} of the redox couple may exhibit little variability. This would support the application of Marcus-type relationships or quantitative structure−property relationship (QSPR) models for the estimation of electron transfer rate constants that are not limited to a single structural family. However, owing to the limited available data on λ_{aq} values for half-cell oxidation reactions, it remains unclear how and whether this apparent constancy can be generalized. Future measurements of aqueous vertical ionization should be conducted for other water-soluble compounds for which accurate one-electron oxidation potentials have been reported in the literature, for example indoles or methoxyphenols, which would enable the determination of additional λ_{aq} values.

Lastly, our study shows that there is room for improvement of the current computational methodology, which left discrepancies of up to 0.26 eV with respect to experimental aqueous photoelectron spectra for the band maximum of the VIE_{aq}. Simulation of the aqueous vertical ionization requires only the sampling of the reduced state potential energy landscape, and thus this calculation is less taxing than the analogous computation of the equilibrium oxidation potential. This avoids the technical complications associated with the simulation of radicals in solution.[105] The treatment of aqueous solvation of organic compounds remains the chief technical limitation for describing aqueous redox processes in silico.

ASSOCIATED CONTENT

Supporting Information

Experimental and computed aqueous microjet photoelectron spectrum of methoxybenzene, convergence of computed VIE_{aq} values with MD simulation time, additional discussions of VIEs of H-bonded complexes and the ODMB conformational analysis, evolution of veratrole alcohol's d_{COCC} dihedrals with simulation time. This material is available free of charge via the Internet at http://pubs.acs.org.

AUTHOR INFORMATION

Corresponding Author

*E-mail: samuel.arey@epfl.ch.

Notes

The authors declare no competing financial interest.

ACKNOWLEDGMENTS

This work was supported by the Swiss National Science Foundation (SNSF) ProDoc TM Grant PDFMP2-123028 and Project Grant 200021-126893. R.S. acknowledges support from the German Research Foundation (SE 2253/1-1). J.J.G. was supported by the U.S. NSF IRFP Award No. 0852999. The computational work was supported by the Swiss National Supercomputing Center (CSCS) and the EPFL centralized HPC facilities. The authors thank the BESSY II staff for assistance. P.R.T. thanks Petr Slavíček for stimulating discussions.

REFERENCES

(1) Li, C.-J.; Chen, L. Organic Chemistry in Water. *Chem. Soc. Rev.* **2006**, *35*, 68−82.

(2) Valko, M.; Leibfritz, D.; Moncol, J.; Cronin, M. T.; Mazur, M.; Telser, J. Free Radicals and Antioxidants in Normal Physiological Functions and Human Disease. *Int. J. Biochem. Cell Biol.* **2007**, *39*, 44−84.

(3) Sharpless, C. M.; Blough, N. V. The Importance of Charge-Transfer Interactions in Determining Chromophoric Dissolved Organic Matter (CDOM) Optical and Photochemical Properties. *Environ. Sci.: Processes Impacts* **2014**, *16*, 654−671.

(4) Schwarzenbach, R.; Gschwend, P.; Imboden, D. *Environmental Organic Chemistry*; John Wiley & Sons, Inc.: Hoboken, N.J., U.S.A., 2003.

(5) von Gunten, U. Ozonation of Drinking Water: Part I. Oxidation Kinetics and Product Formation. *Water Res.* **2003**, *37*, 1443−1467.

(6) von Gunten, U. Ozonation of Drinking Water: Part II. Disinfection and By-Product Formation in Presence of Bromide, Iodide or Chlorine. *Water Res.* **2003**, *37*, 1469−1487.

(7) Deborde, M.; von Gunten, U. Reactions of Chlorine with Inorganic and Organic Compounds During Water Treatment−Kinetics and Mechanisms: A Critical Review. *Water Res.* **2008**, *42*, 13−51.

(8) Jacob, D. J. Heterogeneous Chemistry and Tropospheric Ozone. *Atmos. Environ.* **2000**, *34*, 2131−2159.

(9) Ervens, B.; Turpin, B. J.; Weber, R. J. Secondary Organic Aerosol Formation in Cloud Droplets and Aqueous Particles (aqSOA): a Review of Laboratory, Field and Model Studies. *Atmos. Chem. Phys.* **2011**, *11*, 11069−11102.

(10) Turner, D. W.; Jobory, M. I. A. Determination of Ionization Potentials by Photoelectron Energy Measurement. *J. Chem. Phys.* **1962**, *37*, 3007−3008.

(11) Reinert, F.; Hüfner, S. Photoemission Spectroscopy−from Early Days to Recent Applications. *New J. Phys.* **2005**, *7*, 97.

(12) Winter, B. Liquid Microjet for Photoelectron Spectroscopy. *Nucl. Instr. Meth. Phys. Res. A* **2009**, *601*, 139−150.

(13) Winter, B.; Faubel, M. Photoemission from Liquid Aqueous Solutions. *Chem. Rev.* **2006**, *106*, 1176−1211.

(14) Seidel, R.; Thürmer, S.; Winter, B. Photoelectron Spectroscopy Meets Aqueous Solution: Studies from a Vacuum Liquid Microjet. *J. Phys. Chem. Lett.* **2011**, *2*, 633−641.

(15) Weber, R.; Winter, B.; Schmidt, P. M.; Widdra, W.; Hertel, I. V.; Dittmar, M.; Faubel, M. Photoemission from Aqueous Alkali-Metal-Iodide Salt Solutions Using EUV Synchrotron Radiation. *J. Phys. Chem. B* **2004**, *108*, 4729−4736.

(16) Winter, B.; Weber, R.; Schmidt, P. M.; Hertel, I. V.; Faubel, M.; Vrbka, L.; Jungwirth, P. Molecular Structure of Surface-Active Salt Solutions: Photoelectron Spectroscopy and Molecular Dynamics Simulations of Aqueous Tetrabutylammonium Iodide. *J. Phys. Chem. B* **2004**, *108*, 14558−14564.

(17) Winter, B.; Weber, R.; Hertel, I. V.; Faubel, M.; Jungwirth, P.; Brown, E. C.; Bradforth, S. E. Electron Binding Energies of Aqueous Alkali and Halide Ions: EUV Photoelectron Spectroscopy of Liquid Solutions and Combined Ab Initio and Molecular Dynamics Calculations. *J. Am. Chem. Soc.* **2005**, *127*, 7203−7214.

(18) Winter, B.; Faubel, M.; Hertel, I. V.; Pettenkofer, C.; Bradforth, S. E.; Jagoda-Cwiklik, B.; Cwiklik, L.; Jungwirth, P. Electron Binding Energies of Hydrated H_3O^+ and OH^-: Photoelectron Spectroscopy of Aqueous Acid and Base Solutions Combined with Electronic Structure Calculations. *J. Am. Chem. Soc.* **2006**, *128*, 3864−3865.

(19) Seidel, R.; Faubel, M.; Winter, B.; Blumberger, J. Single-Ion Reorganization Free Energy of Aqueous $Ru(bpy)_3^{2+/3+}$ and $Ru(H_2O)_6^{2+/3+}$ from Photoemission Spectroscopy and Density Functional Molecular Dynamics Simulation. *J. Am. Chem. Soc.* **2009**, *131*, 16127−16137.

(20) Moens, J.; Seidel, R.; Geerlings, P.; Faubel, M.; Winter, B.; Blumberger, J. Energy Levels and Redox Properties of Aqueous $Mn^{2+/3+}$ from Photoemission Spectroscopy and Density Functional Molecular Dynamics Simulation. *J. Phys. Chem. B* **2010**, *114*, 9173−9182.

(21) Pluhařová, E.; Ončák, M.; Seidel, R.; Schroeder, C.; Schroeder, W.; Winter, B.; Bradforth, S. E.; Jungwirth, P.; Slavíček, P. Transforming Anion Instability into Stability: Contrasting Photoionization of Three Protonation Forms of the Phosphate Ion upon Moving into Water. *J. Phys. Chem. B* **2012**, *116*, 13254−13264.

(22) Seidel, R.; Thürmer, S.; Moens, J.; Geerlings, P.; Blumberger, J.; Winter, B. Valence Photoemission Spectra of Aqueous $Fe^{2+/3+}$ and $[Fe(CN)_6]^{4/3}$ and Their Interpretation by DFT Calculations. *J. Phys. Chem. B* **2011**, *115*, 11671−11677.

(23) Thürmer, S.; Seidel, R.; Winter, B.; Ončák, M.; Slavíček, P. Flexible H_2O_2 in Water: Electronic Structure from Photoelectron Spectroscopy and Ab Initio Calculations. *J. Phys. Chem. A* **2011**, *115*, 6239−6249.

(24) Jagoda-Cwiklik, B.; Slavicek, P.; Cwiklik, L.; Nolting, D.; Winter, B.; Jungwirth, P. Ionization of Imidazole in the Gas Phase, Microhydrated Environments, and in Aqueous Solution. *J. Phys. Chem. A* **2008**, *112*, 3499−3505.

(25) Jagoda-Cwiklik, B.; Slavicek, P.; Nolting, D.; Winter, B.; Jungwirth, P. Ionization of Aqueous Cations: Photoelectron Spectroscopy and ab Initio Calculations of Protonated Imidazole. *J. Phys. Chem. B* **2008**, *112*, 7355−7358.

(26) Slavicek, P.; Winter, B.; Faubel, M.; Bradforth, S. E.; Jungwirth, P. Ionization Energies of Aqueous Nucleic Acids: Photoelectron Spectroscopy of Pyrimidine Nucleosides and Ab Initio Calculations. *J. Am. Chem. Soc.* **2009**, *131*, 6460−6467.

(27) Ghosh, D.; Roy, A.; Seidel, R.; Winter, B.; Bradforth, S.; Krylov, A. I. First-Principle Protocol for Calculating Ionization Energies and Redox Potentials of Solvated Molecules and Ions: Theory and Application to Aqueous Phenol and Phenolate. *J. Phys. Chem. B* **2012**, *116*, 7269−7280.

(28) Bartmess, J. E. Thermodynamics of the Electron and the Proton. *J. Phys. Chem.* **1994**, *98*, 6420−6424.

(29) Zhou, H.-X.; Szabo, A. Microscopic Formulation of Marcus Theory of Electron Transfer. *J. Chem. Phys.* **1995**, *103*, 3481−3494.

(30) Adriaanse, C.; Sulpizi, M.; VandeVondele, J.; Sprik, M. The Electron Attachment Energy of the Aqueous Hydroxyl Radical Predicted from the Detachment Energy of the Aqueous Hydroxide Anion. *J. Am. Chem. Soc.* **2009**, *131*, 6046−6047.

(31) Warshel, A. Dynamics of Reactions in Polar Solvents. Semiclassical Trajectory Studies of Electron-Transfer and Proton-Transfer Reactions. *J. Phys. Chem.* **1982**, *86*, 2218−2224.

(32) Blumberger, J.; Sprik, M. In *Computer Simulations in Condensed Matter Systems: From Materials to Chemical Biology, Vol. 2*; Ferrario, M., Ciccotti, G., Binder, K., Eds.; Lecture Notes in Physics; Springer: Berlin; Heidelberg, 2006; Vol. *704*, pp 481−506.

(33) Marcus, R. Chemical and Electrochemical Electron-Transfer Theory. *Annu. Rev. Phys. Chem.* **1964**, *15*, 155−196.

(34) Marcus, R. A. On the Theory of Oxidation-Reduction Reactions Involving Electron Transfer. III. Applications to Data on the Rates of Organic Redox Reactions. *J. Chem. Phys.* **1957**, *26*, 872−877.

(35) Eberson, L. Electron-Transfer Reactions in Organic Chemistry. *Adv. Phys. Org. Chem.* **1982**, *18*, 79−185.

(36) Frisch, M. J.; Trucks, G. W.; Schlegel, H. B.; Scuseria, G. E.; Robb, M. A.; Cheeseman, J. R.; Scalmani, G.; Barone, V.; Mennucci, B.; Petersson, G. A.; et al. *Gaussian09*, Revision B.1; Gaussian Inc.: Wallingford, CT, 2009.

(37) Schwabe, T.; Grimme, S. Double-Hybrid Density Functionals with Long-Range Dispersion Corrections: Higher Accuracy and Extended Applicability. *Phys. Chem. Chem. Phys.* **2007**, *9*, 3397−3406.

(38) Weigend, F.; Ahlrichs, R. Balanced Basis Sets of Split Valence, Triple Zeta Valence and Quadruple Zeta Valence Quality for H to Rn: Design and Assessment of Accuracy. *Phys. Chem. Chem. Phys.* **2005**, *7*, 3297−3305.

(39) Kendall, R. A.; Thom H. Dunning, J.; Harrison, R. J. Electron Affinities of the First-Row Atoms Revisited. Systematic Basis Sets and Wave Functions. *J. Chem. Phys.* **1992**, *96*, 6796−6806.

(40) Krishnan, R.; Binkley, J. S.; Seeger, R.; Pople, J. A. Self-Consistent Molecular Orbital Methods. XX. A Basis Set for Correlated Wave Functions. *J. Chem. Phys.* **1980**, *72*, 650−654.
(41) Jensen, F. *Introduction to Computational Chemistry*; John Wiley & Sons, Inc.: Chichester, U.K., 2007.
(42) Wood, G. P. F.; Radom, L.; Petersson, G. A.; Barnes, E. C.; Frisch, M. J.; John A. Montgomery, J. A Restricted-Open-Shell Complete-Basis-Set Model Chemistry. *J. Chem. Phys.* **2006**, *125*, 094106.
(43) Martin, J. M. L.; de Oliveira, G. Towards Standard Methods for Benchmark Quality Ab Initio Thermochemistry−W1 and W2 Theory. *J. Chem. Phys.* **1999**, *111*, 1843−1856.
(44) Barnes, E. C.; Petersson, G. A.; Montgomery, J. A.; Frisch, M. J.; Martin, J. M. L. Unrestricted Coupled Cluster and Brueckner Doubles Variations of W1 Theory. *J. Chem. Theory Comput.* **2009**, *5*, 2687−2693.
(45) Tentscher, P. R.; Arey, J. S. Geometries and Vibrational Frequencies of Small Radicals: Performance of Coupled Cluster and More Approximate Methods. *J. Chem. Theory Comput.* **2012**, *8*, 2165−2179.
(46) Hill, T. L. In *An Introduction to Statistical Thermodynamics*; Bonner, F. T., Pimentel, G. C., Eds.; Dover Publications Inc.: Mineola, N.Y., U.S.A., 1986.
(47) Barone, V. Anharmonic Vibrational Properties by a Fully Automated Second-Order Perturbative Approach. *J. Chem. Phys.* **2005**, *122*, 014108.
(48) Zhao, Y.; Truhlar, D. G. A New Local Density Functional for Main-Group Thermochemistry, Transition Metal Bonding, Thermochemical Kinetics, and Noncovalent Interactions. *J. Chem. Phys.* **2006**, *125*, 194101.
(49) Marenich, A. V.; Cramer, C. J.; Truhlar, D. G. Universal Solvation Model Based on Solute Electron Density and on a Continuum Model of the Solvent Defined by the Bulk Dielectric Constant and Atomic Surface Tensions. *J. Phys. Chem. B* **2009**, *113*, 6378−6396.
(50) Becke, A. D. A New Mixing of Hartree−Fock and Local Density-Functional Theories. *J. Chem. Phys.* **1993**, *98*, 1372−1377.
(51) Boys, S.; Bernardi, F. The Calculation of Small Molecular Interactions by the Differences of Separate Total Energies. Some Procedures with Reduced Errors. *Mol. Phys.* **1970**, *19*, 553−566.
(52) Tentscher, P. R.; Arey, J. S. On the Nature of Interactions of Radicals with Polar Molecules. *J. Phys. Chem. A* **2013**, *117*, 12560−12568.
(53) Tentscher, P. R.; Arey, J. S. Binding in Radical-Solvent Binary Complexes: Benchmark Energies and Performance of Approximate Methods. *J. Chem. Theory Comput.* **2013**, *9*, 1568−1579.
(54) Case, D. A.; Darden, T. A.; Cheatham, T. E.; Simmerling, C. L.; Wang, J.; Duke, R. E.; Luo, R.; Crowley, M.; Walker, R. C.; Zhang, W.; et al. *AMBER 11*; University of California: San Francisco, CA, 2009.
(55) Wang, J.; Wolf, R. M.; Caldwell, J. W.; Kollman, P. A.; Case, D. A. Development and Testing of a General AMBER Force Field. *J. Comput. Chem.* **2004**, *25*, 1157−1174.
(56) Caldwell, J. W.; Kollman, P. A. Structure and Properties of Neat Liquids Using Nonadditive Molecular Dynamics: Water, Methanol, and N-Methylacetamide. *J. Phys. Chem.* **1995**, *99*, 6208−6219.
(57) Ryckaert, J.-P.; Ciccotti, G.; Berendsen, H. J. Numerical Integration of the Cartesian Equations of Motion of a System with Constraints: Molecular Dynamics of *n*-Alkanes. *J. Comput. Phys.* **1977**, *23*, 327−341.
(58) CP2K; www.cp2k.org, accessed August, 2012.
(59) Grimme, S. Semiempirical GGA-Type Density Functional Constructed with a Long-Range Dispersion Correction. *J. Comput. Chem.* **2006**, *27*, 1787−1799.
(60) Krack, M. Pseudopotentials for H to Kr Optimized for Gradient-Corrected Exchange-Correlation Functionals. *Theor. Chem. Acc.* **2005**, *114*, 145−152.
(61) Lippert, G.; Hutter, J.; Parrinello, M. The Gaussian and Augmented-Plane-Wave Density Functional Method for Ab Initio Molecular Dynamics Simulations. *Theor. Chem. Acc.* **1999**, *103*, 124−140.
(62) VandeVondele, J.; Krack, M.; Mohamed, F.; Parrinello, M.; Chassaing, T.; Hutter, J. Quickstep: Fast and Accurate Density Functional Calculations Using a Mixed Gaussian and Plane Waves Approach. *Comput. Phys. Commun.* **2005**, *167*, 103−128.
(63) Laino, T.; Mohamed, F.; Laio, A.; Parrinello, M. An Efficient Real Space Multigrid QM/MM Electrostatic Coupling. *J. Chem. Theory Comput.* **2005**, *1*, 1176−1184.
(64) Laino, T.; Mohamed, F.; Laio, A.; Parrinello, M. An Efficient Linear-Scaling Electrostatic Coupling for Treating Periodic Boundary Conditions in QM/MM Simulations. *J. Chem. Theory Comput.* **2006**, *2*, 1370−1378.
(65) Kosenkov, D.; Slipchenko, L. V. Solvent Effects on the Electronic Transitions of *p*-Nitroaniline: A QM/EFP Study. *J. Phys. Chem. A* **2011**, *115*, 392−401.
(66) Slipchenko, L. V. Solvation of the Excited States of Chromophores in Polarizable Environment: Orbital Relaxation versus Polarization. *J. Phys. Chem. A* **2010**, *114*, 8824−8830.
(67) Shao, Y.; Molnar, L. F.; Jung, Y.; Kussmann, J.; Ochsenfeld, C.; Brown, S. T.; Gilbert, A. T.; Slipchenko, L. V.; Levchenko, S. V.; O'Neill, D. P.; et al. Advances in Methods and Algorithms in a Modern Quantum Chemistry Program Package. *Phys. Chem. Chem. Phys.* **2006**, *8*, 3172−3191.
(68) Stanton, J. F.; Gauss, J. Analytic Energy Derivatives for Ionized States Described by the Equation-of-Motion Coupled Cluster Method. *J. Chem. Phys.* **1994**, *101*, 8938−8944.
(69) Truhlar, D. G.; Cramer, C. J.; Lewis, A.; Bumpus, J. A. *Correction to J. Chem. Educ.* **2004**, *81*, 596−604; *J. Chem. Educ.* **2007**, *84*, 934.
(70) Zambom, A. Z.; Dias, R. A Review of Kernel Density Estimation with Applications to Econometrics. *International Econometric Review (IER)* **2013**, *5*, 20−42.
(71) Efron, B.; Tibshirani, R. Bootstrap Methods for Standard Errors, Confidence Intervals, and Other Measures of Statistical Accuracy. *Stat. Sci.* **1986**, *1*, 54−75.
(72) Guerard, J. J.; Arey, J. S. Critical Evaluation of Implicit Solvent Models for Predicting Aqueous Oxidation Potentials of Neutral Organic Compounds. *J. Chem. Theory Comput.* **2013**, *9*, 5046−5058.
(73) Linstrom, P., Mallard, W., Eds. *NIST Chemistry WebBook, NIST Standard Reference Database Number 69*; National Institute of Standards and Technology: Gaithersburg MD, 20899, http://webbook.nist.gov (accessed September, 2012).
(74) Schwell, M.; Jochims, H.-W.; Baumgärtel, H.; Leach, S. VUV Photophysics and Dissociative Photoionization of Pyrimidine, Purine, Imidazole and Benzimidazole in the 7−18 eV Photon Energy Range. *Chem. Phys.* **2008**, *353*, 145−162.
(75) Cradock, S.; Findlay, R.; Palmer, M. The Molecular Energy Levels of the Azoles: A Study by Photoelectron Spectroscopy and Ab Initio Molecular Orbital Calculations. *Tetrahedron* **1973**, *29*, 2173−2181.
(76) Klasinc, L.; Ruščič, B.; Kajfež, F.; Šunjić, V. Photoelectron Spectroscopy of the Heterocycles Imidazole and Methylimidazoles. *Int. J. Quantum Chem.* **1978**, *14*, 367−371.
(77) Song, X.; Yang, M.; Davidson, E. R.; Reilly, J. P. Zero Kinetic Energy Photoelectron Spectra of Jet-Cooled Aniline. *J. Chem. Phys.* **1993**, *99*, 3224−3233.
(78) Dopfer, O.; Reiser, G.; Müller-Dethlefs, K.; Schlag, E. W.; Colson, S. D. Zero-Kinetic-Energy Photoelectron Spectroscopy of the Hydrogen-Bonded Phenol−Water Complex. *J. Chem. Phys.* **1994**, *101*, 974−989.
(79) Pradhan, M.; Li, C.; Lin, J. L.; Tzeng, W. B. Mass Analyzed Threshold Ionization Spectroscopy of Anisole Cation and the OCH3 Substitution Effect. *Chem. Phys. Lett.* **2005**, *407*, 100−104.
(80) Choi, S.; Choi, K.-W.; Kim, S. K.; Chung, S.; Lee, S. Vibrational Structures of Dimethyl Sulfide and Ethylene Sulfide Cations Studied by Vacuum-Ultraviolet Mass-Analyzed Threshold Ionization (MATI) Spectroscopy. *J. Phys. Chem. A* **2006**, *110*, 13183−13187.
(81) Choi, K.-W.; Lee, J.-H.; Kim, S. K. Ionization Spectroscopy of a DNA Base- Vacuum-Ultraviolet Mass-Analyzed Threshold Ionization

Spectroscopy of Jet-Cooled Thymine. *J. Am. Chem. Soc.* **2005**, *127*, 15674−15675.
(82) Yang, S. C.; Huang, S. W.; Tzeng, W. B. Rotamers of *o*- and *m*-Dimethoxybenzenes Studied by Mass-Analyzed Threshold Ionization Spectroscopy and Theoretical Calculations. *J. Phys. Chem. A* **2010**, *114*, 11144−11152.
(83) Kim, J. B.; Yacovitch, T. I.; Hock, C.; Neumark, D. M. Slow Photoelectron Velocity-Map Imaging Spectroscopy of the Phenoxide and Thiophenoxide Anions. *Phys. Chem. Chem. Phys.* **2011**, *13*, 17378−17383.
(84) Klasinc, L.; Kovac, B.; Güsten, H. Photoelectron Spectra of Acenes. Electronic Structure and Substituent Effects. *Pure Appl. Chem.* **1983**, *55*, 289−298.
(85) Anderson, G. M.; Kollman, P. A.; Domelsmith, L. N.; Houk, K. N. Methoxy Group Nonplanarity in *o*-Dimethoxybenzenes. Simple Predictive Models for Conformations and Rotational Barriers in Alkoxyaromatics. *J. Am. Chem. Soc.* **1979**, *101*, 2344−2352.
(86) Dorofeeva, O. V.; Shishkov, I. F.; Karasev, N. M.; Vilkov, L. V.; Oberhammer, H. Molecular Structures of 2-Methoxyphenol and 1,2-Dimethoxybenzene as Studied by Gas-Phase Electron Diffraction and Quantum Chemical Calculations. *J. Mol. Struct.* **2009**, *933*, 132−141.
(87) Miller, B. J.; Kjaergaard, H. G.; Hattori, K.; ichi Ishiuchi, S.; Fujii, M. The Most Stable Conformer of Benzyl Alcohol. *Chem. Phys. Lett.* **2008**, *466*, 21−26.
(88) Yurenko, Y. P.; Zhurakivsky, R. O.; Ghomi, M.; Samijlenko, S. P.; Hovorun, D. M. How Many Conformers Determine the Thymidine Low-Temperature Matrix Infrared Spectrum? DFT and MP2 Quantum Chemical Study. *J. Phys. Chem. B* **2007**, *111*, 9655−9663.
(89) As the experimental $VIE_{1,gas}$ band is nongaussian in shape and highly structured, we evaluated the interpeak distance from our computed $VIE_{1,gas}$ and the experimental $VIE_{2,gas}$
(90) Blumberger, J. Free Energies for Biological Electron Transfer from QM/MM Calculation: Method, Application and Critical Assessment. *Phys. Chem. Chem. Phys.* **2008**, *10*, 5651−5667.
(91) Jonsson, M.; Lind, J.; Eriksen, T. E.; Merenyi, G. Redox and Acidity Properties of 4-Substituted Aniline Radical Cations in Water. *J. Am. Chem. Soc.* **1994**, *116*, 1423−1427.
(92) Canonica, S.; Hellrung, B.; Wirz, J. Oxidation of Phenols by Triplet Aromatic Ketones in Aqueous Solution. *J. Phys. Chem. A* **2000**, *104*, 1226−1232.
(93) Jonsson, M.; Lind, J.; Reitberger, T.; Eriksen, T. E.; Merenyi, G. Redox Chemistry of Substituted Benzenes: the One-Electron Reduction Potentials of Methoxy-Substituted Benzene Radical Cations. *J. Phys. Chem.* **1993**, *97*, 11278−11282.
(94) Lind, J.; Shen, X.; Eriksen, T. E.; Merenyi, G. The One-Electron Reduction Potential of 4-Substituted Phenoxyl Radicals in Water. *J. Am. Chem. Soc.* **1990**, *112*, 479−482.
(95) Bietti, M.; Baciocchi, E.; Steenken, S. Lifetime, Reduction Potential and Base-Induced Fragmentation of the Veratryl Alcohol Radical Cation in Aqueous Solution. Pulse Radiolysis Studies on a Ligninase Mediator. *J. Phys. Chem. A* **1998**, *102*, 7337−7342.
(96) Merényi, G.; Lind, J.; Engman, L. The Dimethylhydroxysulfuranyl Radical. *J. Phys. Chem.* **1996**, *100*, 8875−8881.
(97) Thürmer, S.; Seidel, R.; Faubel, M.; Eberhardt, W.; Hemminger, J. C.; Bradforth, S. E.; Winter, B. Photoelectron Angular Distributions from Liquid Water: Effects of Electron Scattering. *Phys. Rev. Lett.* **2013**, *111*, 173005.
(98) Oana, M. C.; Krylov, A. I. Dyson Orbitals for Ionization from the Ground and Electronically Excited States within Equation-of-Motion Coupled-Cluster Formalism: Theory, Implementation, and Examples. *J. Chem. Phys.* **2007**, *127*, 234106−1−14.
(99) Oana, M. C.; Krylov, A. I. Cross Sections and Photoelectron Angular Distributions in Photodetachment from Negative Ions Using Equation-of-Motion Coupled-Cluster Dyson Orbitals. *J. Chem. Phys.* **2009**, *131*, 124114−1−15.
(100) Ghosh, D.; Isayev, O.; Slipchenko, L. V.; Krylov, A. I. Effect of Solvation on the Vertical Ionization Energy of Thymine: From Microhydration to Bulk. *J. Phys. Chem. A* **2011**, *115*, 6028−6038.
(101) Basché, T.; Bräuchle, C.; Voitländer, J. Different Conformations of *ortho*-Dimethoxybenzene as Studied by Phosphorescence spectroscopy. *Chem. Phys. Lett.* **1988**, *144*, 226−230.
(102) Facelli, J. C. Nonplanarity of the Methoxy Groups in *o*-Dimethoxybenzene: Quantum Chemical Calculations of the ^{17}O Chemical Shieldings. *THEOCHEM* **1992**, *276*, 307−313.
(103) Schaefer, T.; Laatikainen, R. The Probable Planarity of 1,2-Dimethoxybenzene in Solution. *Can. J. Chem.* **1983**, *61*, 224−229.
(104) Schaefer, T.; Sebastian, R.; Lemire, A.; Penner, G. H. ^{1}H and ^{13}C NMR Studies of the Conformational Mobility of 1,2-Dimethoxybenzene in Solution. *Can. J. Chem.* **1990**, *68*, 1393−1398.
(105) As the solute is not at equilibrium with its environment, many specifics of ion and radical solvation need not to be considered. For example, severely shortened hydrogen bond distances of acidic protons are absent, and enhanced donor−acceptor properties of radicals[52] are avoided due to the distance of the solvent molecules.